CHALMERS
UNIVERSITY OF TECHNOLOGY

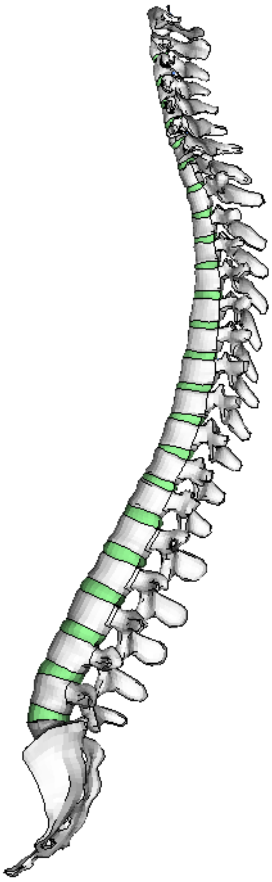

Spinal Curvature Update of the SAFER Human Body Model

A study on the effect of spinal curvature in frontal and run-off road crash scenarios

Master's thesis in Biomedical Engineering

Emmy Alvius & Molly Lundqvist

DEPARTMENT OF MECHANICS AND MARITIME SCIENCES
CHALMERS UNIVERSITY OF TECHNOLOGY
Gothenburg, Sweden 2026
www.chalmers.se

Master's thesis 2026

Spinal Curvature Update of the SAFER Human Body Model

A study on the effect of spinal curvature in frontal and run-off road crash scenarios

Emmy Alvius & Molly Lundqvist

CHALMERS
UNIVERSITY OF TECHNOLOGY

Department of Mechanics and Maritime Sciences
Division of Vehicle Safety
Chalmers University of Technology
Gothenburg, Sweden 2026

Spinal Curvature Update of the SAFER Human Body Model
A study on the effect of spinal curvature in frontal and run-off road crash scenarios
Emmy Alvius & Molly Lundqvist

Supervisor: Jonas Östh, Volvo Car AB
Examiner: Johan Davidsson, Department of Mechanics and Maritime Sciences

Master's Thesis 2026
Department of Mechanics and Maritime Sciences
Division of Vehicle Safety
Chalmers University of Technology
SE-412 96 Gothenburg
Telephone +46 31 772 1000

Cover: The spine of the SAFER HBM.

Typeset in LaTeX
Printed by Chalmers Reproservice
Gothenburg, Sweden 2026

Spinal Curvature Update of the SAFER Human Body Model
A study on the effect of spinal curvature in frontal and run-off road crash scenarios
EMMY ALVIUS & MOLLY LUNDQVIST
Department of Mechanics and Maritime Sciences
Chalmers University of Technology

Abstract

The human body is a complex system made of various tissues, making it a difficult task to model in a biofidelic manner. It is of importance to be able to accurately do this in order to predict the risk of injury when exposed to large magnitudes of acceleration, e.g. in car crashes. Prior research has found that force and moment within the spine have been significant predictors of vertebral body fracture risk. This thesis implemented a spinal curvature from a prediction model, derived from volunteer data, into the SAFER HBM and evaluated its influence on the spine's mechanical response. This was done in two ways: 1) implementing the curvature of the prediction model in the sagittal plane, as well as 2) varying the curvature in the coronal plane, to represent normal variations within the population with the assumption that the human body is not completely symmetrical.
These two alternative models, together with the original SAFER HBM, were applied in paired simulations of six different crash scenarios to investigate whether the mechanical response of the vertebrae differed. The crash scenarios modelled were two frontal crashes of different severity, two oblique crashes of different impact directions as well as two run-off road scenarios with different vehicle roll motions.
When reviewing the updated sagittal spinal curvature, it was seen that the predicted spinal curvature was more straight than the original SAFER HBM, showing reduced lordosis in the upper thoracic spine and reduced kyphosis in the thoracolumbar region. Then, once the updates had been applied into crash simulations, it was noted that the vertebral body trabecular bone inferior-superior strain was affected by the updated curvature, which in its own affects the vertebral body fracture risk. These differences were mainly observed in the run-off road impacts, whereas the variations of frontal impacts did not support the same findings. For these run-off road impacts, it was observed that the compressive forces exerted on the vertebrae were increased with the spinal curvature update. These compressive forces, as well as the flexion of the spine were found to be related to the peak vertebral body trabecular bone inferior-superior strain, in multiple locations in the spine supported by linear regression models. The results of the coronal plane curvature simulations supported the relations between flexion of the spine and compressive strain, as well as between the compressive force and compressive strain.

Keywords: Impact biomechanics, human body model, spinal injuries, spinal curvature, vertebral body fractures, frontal crash, run-off road

Acknowledgements

We want to extend our gratitude to our supervisor **Jonas Östh**, who with his knowledge and time has guided, encouraged and supported us through the entire process of our thesis. Without this support, we would not have learned nearly as much. We also want to thank everyone else in our team Research & Guidelines Protective Safety & Durability at Volvo Cars Safety Centre for contributing to discussions, sharing their work, and welcoming us to the team.
Without the work of **Johan Davidsson** with colleagues, the work of this thesis would not have been possible. Thank you for contributing with valuable insight in discussions throughout the thesis.
Thank you to **Anders Bernhardson** at Ansys for the introductory course to LS-DYNA. This gave us the foundation of knowledge to pursue the thesis work.
We also want to express our gratitude to **Peter Appelgren** at Beta CAE for great technical support regarding the ANSA software, enabling us to get the tools needed to take the step from idea to implementation.
A big thank you to **Wolf Song** with colleagues at TU Delft for sharing their work, giving us a broader perspective of the area.

Emmy Alvius & Molly Lundqvist, Gothenburg, June 2026

List of Acronyms and Abbreviations

Below is the list of acronyms that have been used throughout this thesis listed in alphabetical order:

AR	Aspect Ratio
AIS	Abbreviated Injury Scale
ATD	Anthropomorphic Test Device
CIREN	Crash Injury Research and Engineering Network
DoF	Degrees of Freedom
FE	Finite Element
FEM	Finite Element Modeling
FSU	Functional Spine Unit
HIII	Hybrid III
HIC	Head Injury Criterion
HBM	Human Body Model
IARV	Injury Assessment Reference Value
ISS	Injury Severity Score
MDS	Multi-Dimensional Scaling
MVC	Motor Vehicle Crash
MRI	Magnetic Resonance Imaging
NCAP	New Car Assessment Program
PA	Pelvic Angle
PCA	Principal Component Analysis
PMHS	Post Mortem Human Subject
TUST IBM	Tianjin University of Science & Technology Injury Bionic Model
UMTRI	University of Michigan Transportation Research Institute

Contents

List of Figures

List of Tables

1

Introduction

Motor vehicle crashes (MVCs) with related injuries are still a health problem worldwide [1]. How serious these injuries are, and the consequences thereof, vary. Some injuries lead to long-term impairment, while some could even be fatal. One specific type of injury is spinal injury. Injuries to the spine pose an acute risk for the occupant, but could also lead to long-term impairment in the form of chronic pain and reduced functional capacity [2]. Injuries of this type can arise in different impact scenarios, such as frontal or run-off road crashes [3]. Spinal injuries can be categorized by the location in the spine, that is — cervical spine injuries, thoracic spine injuries, lumbar spine injuries and sacral spine injuries. For the thoracolumbar spine, a typical MVC injury is a compression fracture. In a previous study, cases with injured individuals with Abbreviated Injury Scale 2+ (AIS2+) spinal injury were reviewed and it was reported that while three-point seat-belts were protective against neurologic injury, high overall injury severity and fatality, thoracolumbar fractures were more common than for unbelted occupants [4]. For the lumbar spine, it has previously been stated that compression injuries following axial loading has been seen as a frequently occurring injury [5]. These injuries are the most common AIS2+ injuries to the thoracolumbar spine, with the second most common being wedge fractures. The axial loading is a frequently occurring component in both frontal and run-off road crashes.

It is of great importance to use resources to reduce the number of crashes, but also to reduce the risk of injury in those that still occur, which can be done by designing safe vehicles. To be able to design safe vehicles, it is necessary to know where injury might occur and thus which situations that may pose a danger. Anthropomorphic Test Devices (ATDs) are one tool for studying the human crash response in vehicles, but to provide a more nuanced view of how the body responds to impact, and thus where injury is most likely to occur, Human Body Models (HBMs) can be used. HBMs are unique for their ability to predict the risk of injuries, such as vertebral fractures [6]. For these risks to be estimated correctly, it is needed to adequately model the injury mechanisms and thus the anatomy in a biofidelic manner, i.e. to properly model the spine.

One aspect that needs to be modeled in a biofidelic manner is the positioning of the spine. Depending on how the human (and thus the HBM) is positioned prior to impact, the body moves and interacts with the vehicle in different ways. This is also the case for submodels of the body, such as the spine. It is necessary to accurately position the spine in a crash simulation to be able to predict the related injury risk.

In other words, depending on the curvature of the spine, the risk of injury might vary [3, 7, 8]. Without this being modeled properly, the injury risk in simulation might be over- or underestimated.

1.1 Aim

The aim of this thesis was to evaluate and update the spinal curvature of the SAFER HBM to one representative of a population average male in an upright seated posture, derived from a recent volunteer study. Additionally, the effect of curvature variations on the risk of vertebral body fracture in car crashes was investigated by analyzing the inferior-superior compressive vertebral force, lateral bending and flexion of the spine.

1.1.1 Research questions

- What are the differences between the current spinal curvature of the SAFER HBM and a curvature representing a group of volunteers, in a seated position?
- How can the spinal curvature of the SAFER HBM be updated?
- How does the altered curvature affect the level of compressive strain in the vertebral bodies in simulated car crashes using the updated SAFER HBM?
- How does a curvature in the coronal plane affect the level of compressive strain?

1.2 Delimitations

This thesis was limited to the use of the baseline SAFER HBM 50th percentile male [9] which corresponds to the size of ATDs and HBMs used for car development and testing. However, the HBM can be morphed into other shapes and sizes, creating the possibility of broadening the usability.

The orientation of the pelvis in the SAFER HBM,based on other datasets [10], was desired to be kept fixed, which meant that no update to the angle between vertebra L5 and sacrum was possible. This resulted in changes to the curvature of the spine between the C3—L4 vertebrae. It shall also be noted that no head rotational metric was used during

Other than the delimitations, this thesis was also limited to numerical simulations with the SAFER HBM and versions with updated spinal curvature.

2

Background

The human spine can be divided into the cervical, thoracic and lumbar spine, supported by the sacrum and coccyx [11]. The spine is characterized by its curved appearance, that is of lordotic (cervical and lumbar spine) as well as kyphotic (thoracic spine) nature, Figure 2.2. The cervical spine consist of vertebrae C1—C7, the thoracic spine of vertebrae T1—T12 and the lumbar spine of vertebrae L1—L5. Between every vertebrae from C2 to sacrum, there are intervertebral discs. The intervertebral discs are comprised of the nucleus pulposus, which is the inner part of the disc, and the outer part, the annulus fibrosus [12]. The nucleus pulposus has viscous properties that enable load distribution in the disc, with extracellular matrix that maintain the structural properties of the nucleus. The annulus fibrosus is the outer layer of the disc, made out of a fibrous material that comprises sheets mainly consisting of collagen, creating a structure that is able to sustain multidirectional loads because of alternating fiber orientation. The intervertebral discs protect the integrity of the vertebrae since they absorb and distribute load through the entire spine.

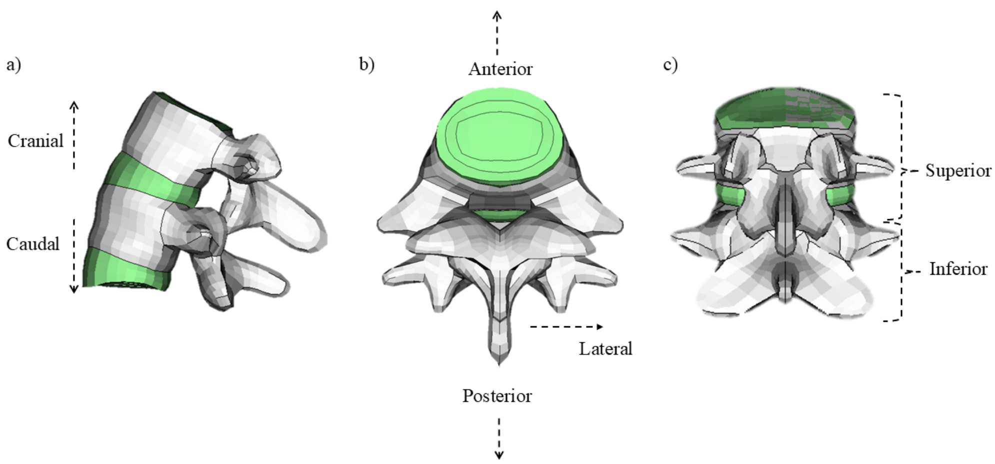

Figure 2.1: Anatomical directions with regards to a functional spine unit (FSU). An FSU in the a) sagittal plane, displaying the cranial and caudal direction, b) transversal plane, displaying the anterior, inferior and lateral direction, c) coronal plane, displaying the superior and inferior vertebra in an FSU.

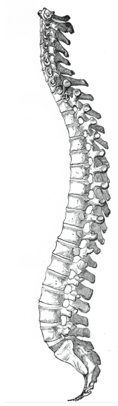

Figure 2.2: The spine in the sagittal plane. Adapted from [13] in compliance with CC0.

The vertebrae (except C1) have a cylindrical body, consisting of trabecular bone covered by cortical bone [11]. The circular void, the vertebral foramen, visualized in Figure 2.3 is where the spinal cord is positioned. The vertebrae have a vertebral lamina, a spinous process and transverse processes. Muscles and ligaments attach to the processes.

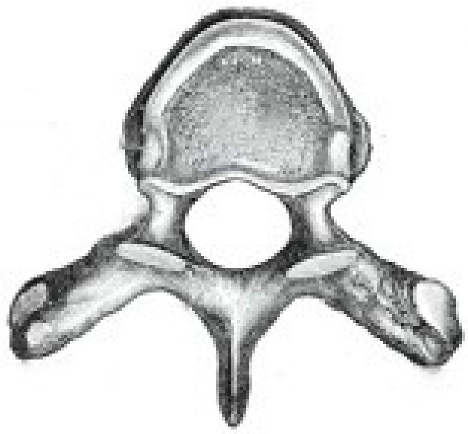

Figure 2.3: A thoracic vertebra in the transversal plane. Adapted from [13] in compliance with CC0.

The vertebrae in the cervical spine are smaller than those in the thoracic and lumbar spine. C1 and C2 differ somewhat anatomically from the other cervical vertebrae, together they form the atlantoaxial joint [11]. Vertebrae C3—C6 are similar in shape with relatively small vertebral bodies [13]. Vertebra C7, also known as vertebra prominens, mainly differ from the other cervical vertebrae through its pronounced spinous process. The transverse processes of C7 are also of larger size than in the other cervical vertebrae.

The thoracic vertebrae are smaller than lumbar vertebrae, but larger than cervical vertebrae [13]. Vertebra T1 is the smallest thoracic vertebra, thereafter the size increases caudally. The thoracic vertebrae have facet joints on the transverse processes where the ribs are connected to the vertebral body, which is how the thoracic vertebrae differ from the cervical and lumbar. The lamina of the thoracic vertebral body is thick and overlaps the inferior vertebra's lamina.

The lumbar vertebrae are the largest, with strong laminae that is relatively short and wide [13]. L5 differ from the other lumbar vertebrae, since it is the largest vertebrae in the cervical, thoracic and lumbar spine with a small spinous process. The most caudal lumbar vertebra is connected through the sacrovertebral joint to the sacral vertebra, also known as S1. S1 is a large, triangular bone, where the coccyx is attached at the end of the spine.

2.1 Injury Severity and Mechanisms

The severity of injuries are usually classified with the Abbreviated Injury Scale (AIS) score on a scale of 1—6, where AIS1 is the least severe and AIS6 the most severe. Regarding spinal injuries, an AIS1 injury is e.g. a contusion of muscle, an AIS2 injury could be a disc herniation or vertebral body fracture in the lumbar spine, while an AIS3 could be a major laceration of a vertebral artery [11].

The loading to the spine causing injuries can be of the characteristics; compression, tension, shear, flexion moment and/or extension moment [11]. A combination of these mechanisms, that could result in spinal injuries are; compression-flexion, compression-extension, tension-flexion, lateral bending or tension-extension, Figure 2.4.

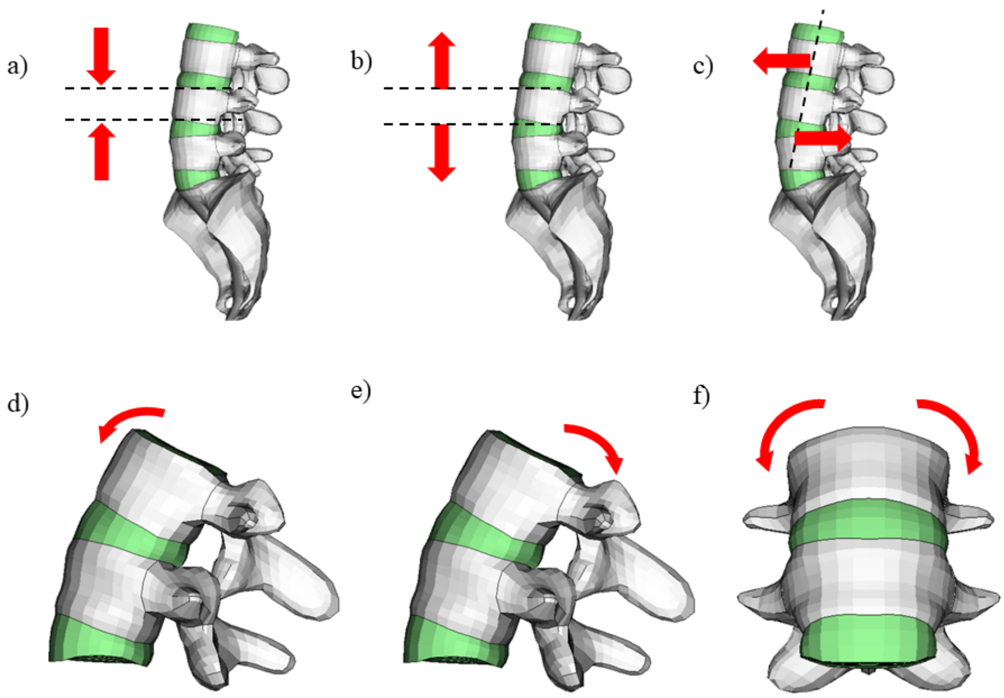

Figure 2.4: a) Compression. b) Tension. c) Shearing. d) Extension. e) Flexion. f) Lateral bending.

2.2 SAFER HBM

The SAFER HBM is developed at the SAFER Vehicle and Traffic Safety Centre at Chalmers University of Technology with core contributors being Autoliv, Chalmers and Volvo Cars [14]. The goal of the SAFER HBM is to have an "omnidirectional, tunable and scalable HBM capable of injury risk and biofidelic kinematics prediction in high-g as well as low-g events". The geometry of the SAFER HBM vertebrae and discs were originally based on an average sized female, and was morphed to fit the 50th percentile male HBM, without altering the curvature. The current spinal curvature of the SAFER HBM v12 is the result of previous model versions, a statistical shape model used for the rib cage [14] and the pelvis that is positioned with a Pelvic Angle (PA) of 45° [9], as defined in [15], Figure 2.6.

2.3 Prior Research

Previous research on spinal curvature for car occupants has focused on measuring the position of the spine of seated occupants and simulations of for instance cervical spine responses in rear-end impacts.

2.3.1 Studying and Modeling the Spinal Curvature

There are examples where the curvature of the spine of HBMs has been altered in the past, such as the Tianjin University of Science & Technology Injury Bionic Models (TUST IBMs), including a 50th percentile male (TUST IBMs M50) [16]. In the publication, the model with original curvature of the spine (M50-D-U) was compared to the same model with adjusted curvature of the spine (M50-D). The spine of the TUST IBM M50 has been curved according to the physiological curvature of the human spine with the lordotic and kyphotic segments by extracting the physiological curvature while seated in a driving position. The model was validated by using Post Mortem Human Subject (PMHS) sled tests. The changes resulted in the IBM hitting the backrest at an earlier time than for the case with original curvature of the spine (at 120 ms instead of at 150 ms), amongst other findings. It was concluded that all of the injury indexes were higher for the adjusted spine (M50-D) than for the original spinal curvature (M50-D-U), indicating that the original curvature underestimated the injury risk.

The spinal position when seated in a car seat has also been studied by using open Magnetic Resonance Imaging (MRI), Figure 2.5 [17].

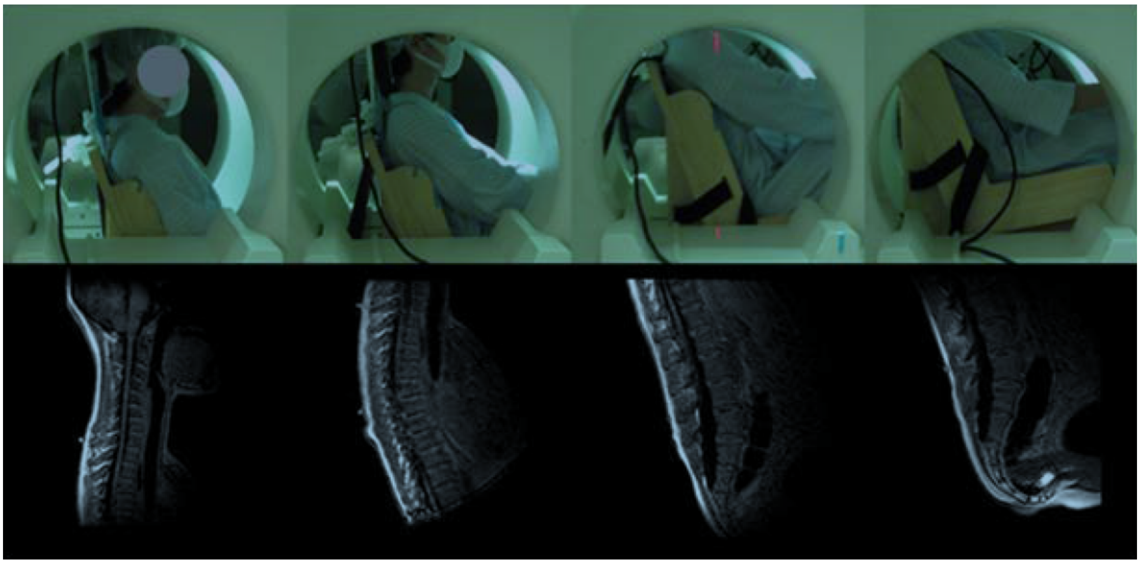

Figure 2.5: Setup and MRI by Sato et al. Image adapted from [17].

In this particular study, differences between male and female subjects were observed regarding the kyphosis and lordosis of the spine. The data was collected from 15 volunteers, seven male and eight female. To be able to investigate the alignment patterns, Multi-Dimensional Scaling (MDS) was used, where the distance between two subjects was expressed as the sum of squares of Euclidian pairwise differences between two corresponding vertebrae. The first MDS dimension was interpreted as a shape factor for the entire spine, due to the combination of degree of the thoracic kyphosis and curvature of the spinal alignment, and was found not statistically significant. The second shape factor for the whole spine alignment was the second MDS dimension, which indicated the position of the thoracolumbar region and was found statistically significant. The explanation to why the first was deemed not statistically significant was due to the limited number of volunteers. It was concluded that there were observed differences in spinal curvature related to sex, as well as patterns in cervical spine alignment in relation to the degree of thoracic kyphosis.

To measure the position of the entire spine in seated positions, a study was done in which reference points were marked on the skin (spinous processes on vertebrae C4 —T10, pelvis, scapula and skull) and documented on a smaller population (21 volunteers) [18]. This data, containing angles between each vertebra and normalized distances between markers were used to construct statistical models of the posture.

2.3.2 Additional Models for Comparison

During the 1980s, the study "Development of Anthropometrically Based Design Specifications for an Advanced Adult Anthropomorphic Dummy Family." was conducted at the University of Michigan Transportation Research Institute (UMTRI) [19]. The results of this study included the mid-sized male dummy, which is commonly referred to as the 50th percentile male dummy [20]. The size of the dummies were based on U.S. population survey data from 1971-1974 as well as consideration being taken to the population of injured occupants. The spinal curvature of the dummy family was based on the seated posture of volunteers.

A recent study conducted at the Delft University of Technology (TU Delft) by Bokdam et al. investigated the difference in seating posture in two seated positions [21]. Since the technical development is moving towards autonomous vehicles, the seating position was evaluated by two differently angled setups for a comparison between an upright and reclined position. The objectives were to investigate the human back shape in seated positions and to evaluate whether it was possible to incorporate it into non-driving related activities. The first driving posture was a 25° backrest angle with a seat pan angle of 15°. The different seating positions mainly affected the curvature of the lumbar spine. To simulate driving posture for the 25° backrest angle, the volunteers were instructed to look at a fixed point in front of them. The positional measurements started at C7 until a u-slot of the backrest used was reached. It was concluded that there were differences in back contours between the two backrest options, where the driving position produced a flatter back contour than the reclined posture.

The curvature of the spine has also been studied by defining parameters based on the angle between different vertebrae, in order to study the kyphosis and lordosis of segments of the spine, Figure 2.6 [15].

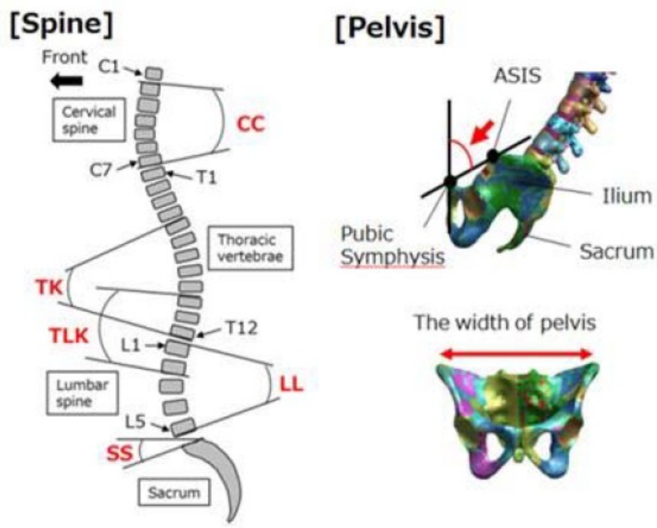

Figure 2.6: Angles and measurements according to Izumiyama et al. Image adapted from [15].

These parameters were the cervical curvature (angle between vertebrae C2 and C7), the thoracic kyphosis (angle between vertebrae T5 and T12), the thoracolumbar kyphosis (angle between vertebrae T10 and L2), the lumbar lordosis (angle between vertebrae L1 and L5), the sacral slope (angle between the sacrum and the horizontal line), the PA (pubic symphysis to the anterior superior iliac spine) and the width of the pelvis defined as the distance between the left and the right ilium, Figure 2.6. This definition of PA is as mentioned how the PA was defined in SAFER HBM v12 [9], and how PA is defined in this thesis.

2.3.3 Injury Risk and Spinal Curvature

The spine protects the spinal cord inside the vertebral foramen, has the function of sustaining loads and acts as structural support to the soft tissues of the body. It can transfer movements and handle bending moments between the upper and lower part of the body [22]. The spinal curvature affects the biomechanical properties of the spine [3].

In a research project investigating factors that could influence the lumbar spine injury risk in frontal crashes, three parametric studies were conducted [8]. A validated model of a vehicle that was available on the US market was used, and the simulations were carried out using a model of the Hybrid III (HIII) 50th percentile male. The 56 km/h US New Car Assessment Program (NCAP) frontal crash test was utilized. The three studies focused on crash conditions, independent effect of design parameters (such as seat design and occupant posture) and the relative sensitivity and statistical significance of the parameters effect on the injury risk of the lumbar spine. The authors found that the variables that had the greatest effect on force in the lumbar spine was crash pulse, seat design (with a focus on the anti-submarining features) and occupant posture. Lumbar spine fractures were concluded to be more common in new vehicle models than old, in frontal crashes. It was argued that this, at least partially, was a result of common anti-submarining functions of the seat. Systems such as knee restraints that decreases submarining increased loads in the lumbar spine. When decreasing this type of restraint, and thus increasing the risk for submarining, the forces in the lumbar spine decreased (4.5 kN to 2.75 kN). This creates a need to account for the axial forces in the lumbar spine when designing safety functions to reduce submarining.

An added pitch angle was also seen to increase the lumbar spine forces (4.5 kN to 6.5 kN) while other metrics such as Head Injury Criterion (HIC) and N_{ij} Injury Criterion were reduced for that alteration [8]. HIC is a measure to quantify risk of skull fracture based on translational acceleration, and is the most commonly used criterion for head injury [11]. Finally, a severe pulse with early peak also increased the load in the lumbar spine, a finding that was consequent with the impact on the metrics HIC and N_{ij} etc. The authors noted in the end of the report that there are limitations of the HIII model, for example the fact that the thoracic spine is a rigid box and the lumbar spine has limited flexibility.

Another study conducted laboratory experiments with 26 PMHS lumbar spines in order to determine how the spinal position affected the injury outcome [23]. It was concluded that the position of the lumbar spine affects how loads are distributed and would thus affect the injury risk. The study was conducted with a military setting in mind. The experiments were performed using a drop tower, where the spine was positioned with a curvature that it naturally "positioned itself in". A mass was added cranially to simulate the weight of the upper body (of a 50th percentile male). The spines were dropped at different heights using gravity as the driving force, and then stopped by foam that was placed beneath. The acceleration, force and moment were measured and the spine was documented using x-ray (before and after the experiment). To conclude, it was stated that the initial hypothesis was proved, i.e., the degree of lordotic curvature did affect the injury outcome. For example, a larger Cobb angle implied greater risk for hyperextension fractures. In comparison, a smaller Cobb angle implied larger risk for burst fractures. It was concluded that a spine in a straighter position was more prone to sustaining fractures to the vertebral body, whilst a spine with a more lordotic curvature tended to sustain fractures to the posterior elements of the vertebrae. This suggests that it matters how the spine is positioned in a loading case.

2.3.4 Impact Scenarios

Vertical loading is a common cause of compression fractures to the spine [24], and there have been studies implying that the most common load cases where this loading occur are run-off road scenarios as well as frontal impacts [3, 24]. When analyzing AIS2+ thoracolumbar spine injuries in real crash data from Volvo cars model year 1999—2013, the most common impacts were frontal and the most common fractures were compression fractures [24]. It was also concluded that it was most common to obtain injury in the area between the thoracic and lumbar spine (in the case of a spinal injury), most frequently at L1 and in the mid-thoracic spine. The posture and flexion of the spine affected the injury outcome in some cases, where injuries often arose from hyper-flexion of the upper body. The authors presented the conclusion that the spinal position was of importance.

The common fracture locations were supported by another study, concluding that over half of the occupants in frontal impacts with thoracolumbar fractures in the Crash Injury Research and Engineering Network (CIREN) database were at level T10 or below [25], with the most common fracture sites being T12 or L1. At L1, the most common fractures were wedge fractures, while burst fractures were most often found in T12, L1 or L5.

Another study concluded that run-off road scenarios were the most common loading case, followed by frontal impacts when reviewing real crash data from Volvo cars during 1991—2005. During impact, spinal injuries, such as vertebral fractures, due to vertical loading could be observed [26]. To address vertical occupant loading in car crashes, test methods were developed aiming to reduce such loads and to evaluate possible countermeasures, since there was no pre-existing standardized test method. The test methods investigated were complete vehicle test on track and rig tests. A moveable covered test track with a semi-directional electrical propulsion system was used from where the car was launched into different run-off road scenarios (e.g. “Ditch”) for complete vehicle tests. The results of the tests constitute that vertical acceleration of the pelvis can be reduced by adding deformation elements in the seat [26]. For future research, it was desired to evaluate the most durable spinal posture, since it was previously stated that the curvature of the spine had an impact on the lumbar and thoracic injury tolerances during axial loading [26, 27].

2.3.5 Coronal Plane Curvature

The spinal curvature is often discussed in terms of lordosis and kyphosis in the sagittal plane, Figure 2.1. However, there are also different curvatures in the coronal plane, most commonly known as scoliosis. Clinically, the definition of scoliosis is based on the Cobb angle and ranges from mild to severe depending on the magnitude of the angle [28], Figure 2.7. Mild scoliosis is defined as a 10—20° angle, moderate as 20—40° and severe as 40°<.

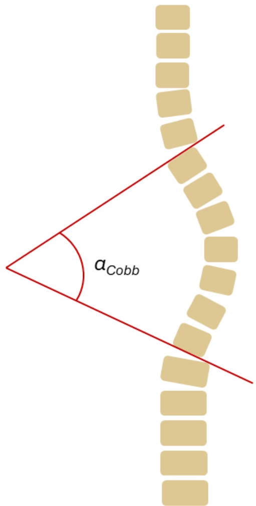

Figure 2.7: The Cobb angle between vertebra T6 and T11.

The Cobb angle is calculated between the top of the most tilted vertebra and the bottom of the most tilted vertebra, above and below the curve's apex respectively, which is how the Cobb angle is defined in this thesis. A curvature in the coronal plane, with a Cobb angle of <10° is classified as a normal spinal curve and not diagnosed as scoliosis. Since the Cobb angle is usually measured when a clinician suspects a scoliosis diagnosis, data regarding the population without suspected scoliosis is sparse. A recent study reviewed two datasets created for retrospective validation of deep learning neural networks, where 67 out of the 345 patients had no angle annotation, or an angle <10° [29]. The global prevalence of scoliosis has previously been estimated to 1.65% [30].

fun

3
Methods

The spinal curvature prediction model used in this thesis was based on data collected from volunteers through palpation and ultrasound measurements [31]. Additional models were considered in the thesis [20, 21, 15].

3.1 Volunteer Data

The data primarily used in this thesis was recorded by Davidsson et al. at Chalmers University of Technology in Gothenburg, Sweden [31]. This data set was comprised of two subsets, recordings of the skin back contour of each volunteer, and ultrasound recordings of the distance from the skin to the lamina of the vertebrae. The 61 volunteers, 31 male and 30 female, were seated in a Volvo car seat. To extract the external shape of the volunteers' back, 10 pins were inserted through the back rest of the seat, palpating the skin where they made contact, Figure 3.1. For these skin locations, x and z coordinates were estimated as well as the skin location of vertebra C3, C5 and C7. The seat deformation for each volunteer was also recorded, since this contributed to a difference in relative position to each pin location with regards to the seat pan in x and z direction, which was different for each volunteer. Other data that were estimated were head center of gravity, as well as the location of the knee, shoulder, trochanter, wrist, elbow and ankle.

Figure 3.1: The setup for data collection from the volunteer study [31].

The ultrasound recordings were conducted with the purpose of measuring the distance to the lamina of the vertebrae from the skin. The ultrasound data together with film marker data together formed an estimate of x and z coordinates for the location of every other vertebra; C3, C5, C7, T2, T4, T6, T8, T10, T12, L2, L4 and S1. The probe was placed approximately in a perpendicular manner on the skin at the locations desired. For the cervical vertebrae, the location of measurement was at the lowest part of the lamina approximately 16 mm lateral of the mid sagittal plane. For the thoracic vertebrae, the measurements were also taken at the lowest part of the lamina but at approximately 20 mm lateral of the mid sagittal plane. For the lumbar vertebrae, the probe was directed at the middle or slightly below the middle of the lamina, approximately 20 mm lateral of the mid sagittal plane. For the sacrum (S1), the probe was directed at the bony surface right or left of the medial sacral crest.

In this volunteer study, measurements were taken in both an upright and reclined seated position. For this thesis, the measurements recorded in an upright seated position, with the seat back angle providing for a 25° angle in the H-point tool, were of interest. Descriptive data were collected for the volunteers, such as sex (M/F), stature (cm), weight (kg) and age (year), 3.1.

Table 3.1: Descriptive data from the volunteer study.

	Min	Mean	Median	Max
Age (year)	16	43	45	66
Weight (kg)	50	76	75	105
Stature (cm)	158	176	174	195

For the purpose of this thesis, it was also necessary to address the coordinate system and reference points used in the data collection. The reference point of these measurements was a rear reference marker that was placed at a location (x, z) behind the seat. The distance to seat back recliner and H-point was recorded, amongst other parameters. From the data recorded, a prediction model based on Principal Component Analysis (PCA) modes was created. This model is what will be referred to as the prediction model in this thesis, if nothing else is specified.

3.2 Additional Models for Comparison

As a way of comparing the prediction model utilized in this thesis, a predictive model by Bokdam et al. was accessed [21]. This model was a reconstruction based on PCA, described in Section 2.3.1.

Other than the Bokdam et al. model, the spinal curvature derived in the study from UMTRI [20] and the average male curvature presented by Izumiyama et al. [15], were also used as sources of comparison, Appendix A. The spinal curvature of the UMTRI model is specified in coordinates for joints between vertebrae instead of coordinates for vertebrae location.

3.3 Comparison of Spinal Curvature

Before updating the spinal curvature of the SAFER HBM, a comparison of the current curvature and the prediction model was executed, both for the lamina line and skin back contour. Additionally, the model by Bokdam et al. [21] was also included as a comparison, as well as the UMTRI model [20] and Izumiyama et al. average male [15], Chapter 4.

To be able to visualize the curvatures, lamina (and skin back) coordinates were retrieved from the SAFER HBM in an unloaded state (not in equilibrium), in approximately the same locations as where measurements were taken on the volunteers. In chapter 4, the curvatures are shifted to be aligned with each other at the L4 or S1 vertebra solely for the purpose of visualization, i.e. not used in the actual spinal curvature update.

3.3.1 Skin to Lamina Distance

In addition to the comparison of lamina line curvature, it was of interest to examine the skin to lamina distance. This was conducted by calculating the distance in x-direction for the SAFER and prediction model respectively. For these measurements in the SAFER HBM, the distance between the locations from which the lamina line was derived from, and the outermost point of the skin was used, Figure 3.2.

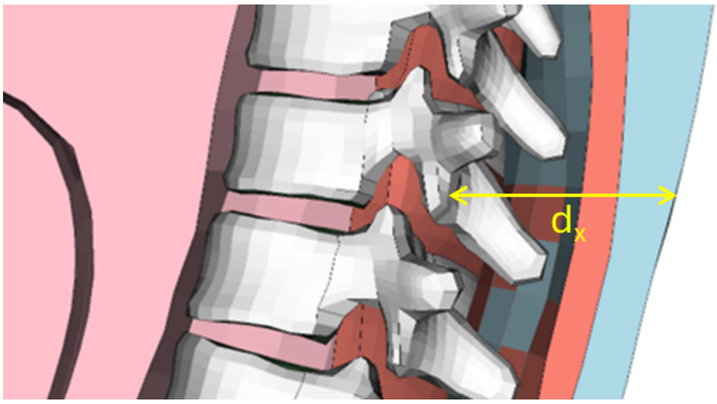

Figure 3.2: Measurement method of skin to lamina distance.

3.3.2 Angle Differences

To quantify the differences between curvatures, it was decided to calculate the angle difference for each vertebrae pair, i.e. the interval between every other vertebra. This was done by extracting the coordinates x, z for two adjacent (measured) vertebrae, e.g. L4 and L2.

When defining the position of the vertebrae in the SAFER HBM, it became apparent that some of the vertebrae were too narrow to extract coordinates at the same locations as Davidsson et al. [31] did in the volunteer study. The solution to this became to extract coordinates as far out laterally as possible on the lamina, Figure 3.3.

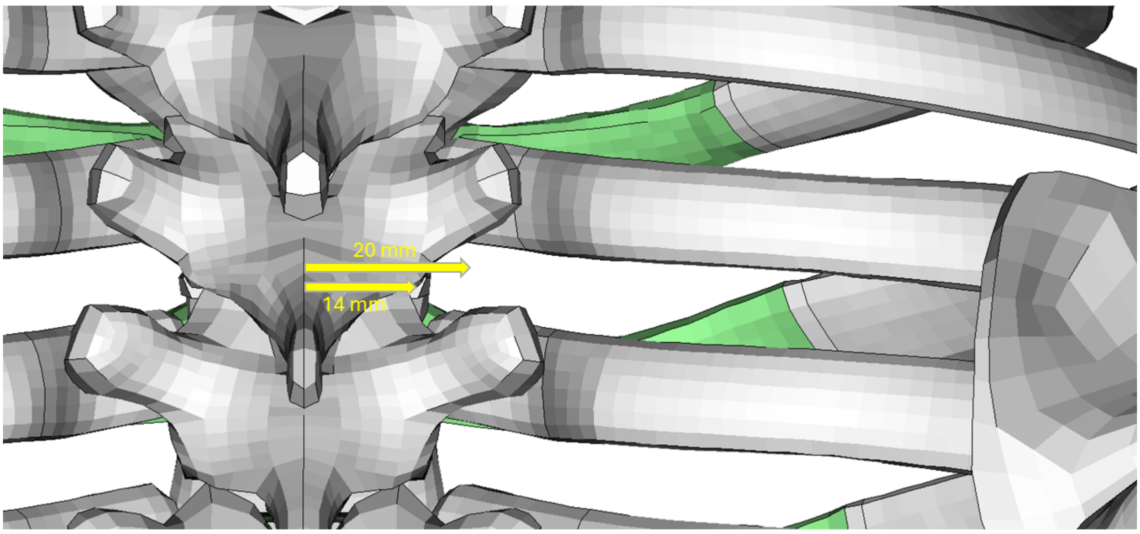

Figure 3.3: Definition of lamina position in the SAFER HBM (vertebra T4).

For this angle calculation, a vertical line that visualizes the y axis was visually inserted in the location of the inferior vertebra, e.g. L4, Figure 3.4. The curvature to the next vertebra (the superior of the two), in this example L2, was approximated with a straight line. Then, the slope of the line joining the two vertebrae was calculated, Equation 3.1, where x_{dist}, z_{dist} is the difference in x and z coordinates respectively from the inferior and the superior vertebra. The result of Equation 3.1 was inserted into Equation 3.2 to acquire the angle between the vertical axis and the line between the vertebrae pair. This was done for both the SAFER HBM and the prediction model. The angle difference, $\Delta\alpha$, was derived by subtracting the prediction angle with the corresponding SAFER HBM angle.

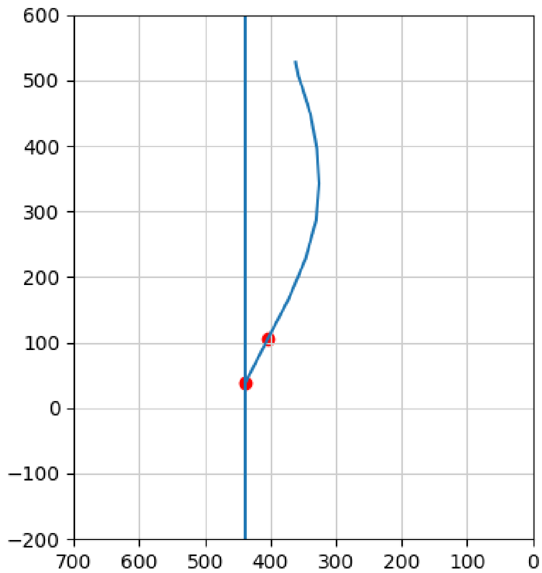

Figure 3.4: Visualization of setup for angle calculation between a vertebrae pair.

$$arg = x_{dist}/z_{dist} \tag{3.1}$$

$$angle = arctan(arg) * 180/\pi \tag{3.2}$$

3.4 Updating the Curvature

The spinal curvature update of the SAFER HBM was performed in two steps. First by rotating every other vertebra with the corresponding $\Delta\alpha$ around the x axis, to create a target position of the spine. Then, the SAFER HBM was simulated into this desired position by pulling the spine into place.

The rotation of the vertebrae was executed using the HBM Articulation tool in ANSA v2025.2.0 (BETA CAE Systems, Luzern, Switzerland) was used. This tool enables rotation of each vertebra around its center of rotation. This function was used for the purpose of rotating the vertebrae around the y axis, and thus altering the curvature in the sagittal plane. Using the $\Delta\alpha$ derived in Section 3.3.2, the vertebrae were rotated one by one, starting in vertebra L4 continuing in cranial order. After applying the rotation to one vertebra, the software morphed the surrounding tissue to comply with the updates. After the morphing, the node file, and thus the position of each vertebra, was extracted and the angles $\Delta\alpha$, were recalculated, resulting in the dependent angle change for the next vertebra.

A change in position of one vertebra would affect the position of the adjacent vertebrae, given that the vertebrae are all connected through the spine. This meant that the exact prediction model curvature was not attained by changing the positions of the vertebrae by rotating with $\Delta\alpha$ once, since the rotation of one superior vertebra would change the position of an inferior vertebra slightly. Therefore, this became an iterative process and the vertebrae positions (in terms of rotation around the y axis) were changed multiple times until an acceptable error range of $\pm 0.5°$ was attained. This resulted in a target positioning of the spine.

To implement the updated position of the spine into the SAFER HBM, the resulting nodes from the articulations were saved as a kinetic position to use as input in the ANSA HBM Marionette tool. Using this tool, it was possible to simulate the HBM into position by applying beams in each location where changes had been made to the position. The applied positioning was displacement based, using 10 kN/mm beams to pull the spine of the HBM into the target position, and the bones were kept rigid. To enable the HBM to move into position, the ribcage structure as a whole, as well as the scapulas and clavicles were allowed to move. The position of the hands were kept fixed as in the original version of the SAFER HBM, as well as the lower extremities, whilst the head was allowed to translate backwards 14 mm to comply with the position of vertebra C3, to avoid any unnatural bending in the atlantoaxial joint. After the spinal position had been implemented, the model quality was checked by analyzing the aspect ratio (AR), Element Jacobian, warping and skewness.

3.4.1 Coronal Plane Curvature

Since the human body is a three-dimensional object, it can bend in more planes than just the sagittal plane. Therefore, it was desired to also vary the curvature in the coronal plane, to one that would represent a normal variation within the population. The aim was to attempt to introduce a Cobb angle, α_{Cobb} in the coronal plane, of less than 10°, given that it was the threshold of what would be considered scoliosis. To determine and implement the curvature in the coronal plane, α_{Cobb} was derived as in Figure 2.7. Nodes were selected to create the guiding lines (colored red, Figure 2.7) on the superior side of the vertebral body for the most cranial vertebra, in the desired area of the spine, and on the inferior side of the most caudal vertebra.

α_{Cobb} was introduced between vertebra T6 (most cranial) and T11 (most caudal) with a magnitude of 9°, in a right curve if observing the spine posteriorly. To do this, the vertebral bodies of vertebra T1 to L5 were isolated, Figure 3.5. The Cobb angle was implemented in the same way as the rotations in the sagittal plane, using the Articulation tool in ANSA, with rotation around the x axis instead. To achieve the 9° Cobb angle, vertebra T6 and T11 were rotated around the x axis by 9°each, but with opposite signs. When simulating the kinetic position using the Marionette tool, the hands, lower extremities and head were kept fixed.

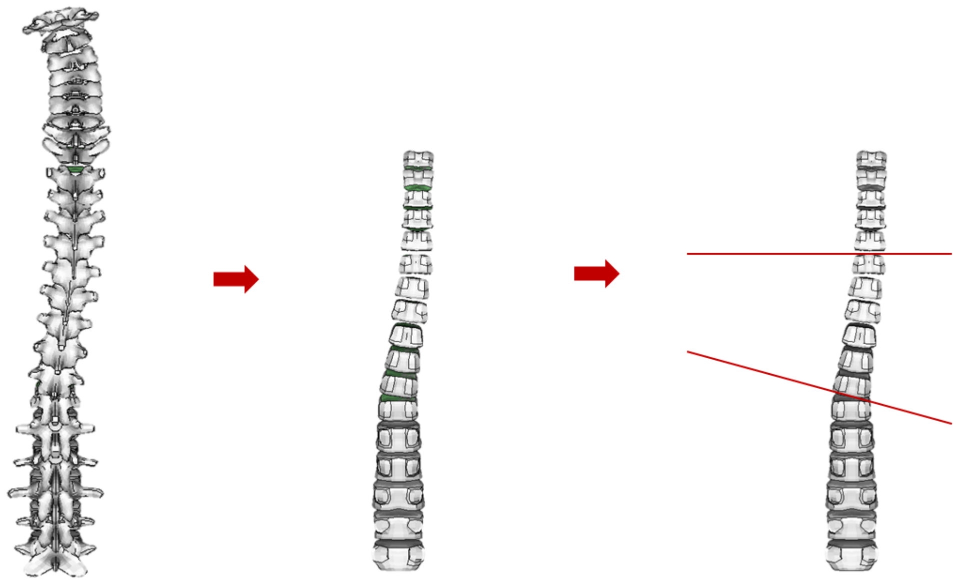

Figure 3.5: Defining the Cobb angle between vertebra T6 and T11.

3.4.2 FE Model Quality

Modeling structures using Finite Element Modeling (FEM) requires that an FE mesh is created for the discretization, associated with the meshing is a number of quality criteria. Previously, it has been reported that developers of FE models do not systematically report the model quality [32], which is needed in order to make the appropriate conclusions from the result that the model produces. Quality issues usually involve the shape of elements in the mesh as well as the number of elements in the mesh. It is generally agreed on that "an optimal mesh density exists that provides the most accurate solution with the smallest possible number of elements" [32].

To perform a mesh quality assessment, metrics such as the AR and Element Jacobians can be utilized. For hexahedral elements, AR is the longest edge divided by the shortest edge of an element. It is desired to have an AR close to 1, an acceptable AR would for instance be an AR of 1—3 [32]. It is however agreed on, when modeling thin and curvy structures such as human cortical bone, that it is acceptable to have a portion of up to 5% of the elements with a relatively higher AR. Values as high as an AR of 23 have been accepted in the past [32, 33]. To evaluate the volume distortion from the optimal shape of an element, the Element Jacobian represents the determinant of the Jacobian matrix. It has previously been suggested that three criteria can be assessed to determine whether the volume distortion is acceptable [32]: it should be a positive value [34, 35], greater than 0.2 in magnitude [33, 36, 37] and less than 5% should have a magnitude lower than 0.7 [38]. Other related metrics are skewness and warping [39].

The model quality was assessed by evaluating the distribution of (shell and solid) elements, as well as comparing the element with the most extreme value regarding the four metrics previously presented.

3.5 Application Study

To apply the variations of the spinal curvature and thus evaluate what effects the updates had, an application study was conducted using META v24.1.6 (BETA CAE Systems, Luzern, Switzerland). It was decided to perform paired simulations which means that for every impact case, three simulations were run, one baseline curvature simulation and two updated curvature simulations. The baseline simulation, using the original SAFER HBM with original spinal curvature, the updated simulation which was run with the SAFER HBM with the updated spinal curvature and lastly the coronal plane curvature. All simulations were conducted for both the driver (position 1) and the front seat passenger (position 3), using an interior sled model of an SUV and the Volvo SPA seats, which was the same car seat as used in the volunteer study that the prediction model by Davidsson et al. was based on [31].

The simulations conducted were a car to car full frontal impact in 35 km/h, varied with an angle change to also create two oblique car to car cases (0° and ±20°), a full frontal car to car impact in 56 km/h and two run-off road scenarios, Table 3.2 and Figure 3.6.

Table 3.2: Simulation matrix.

Sim.	Crash Pulse	Curvature	Total Sim. Time (ms)
1	35 km/h (0°)	Original	150
2		Updated	
3		Coronal plane	
4	56 km/h (0°)	Original	150
5		Updated	
6		Coronal plane	
7	35 km/h (-20°)	Original	150
8		Updated	
9		Coronal plane	
10	35 km/h (20°)	Original	150
11		Updated	
12		Coronal plane	
13	Run-off Road (1)	Original	200
14		Updated	
15		Coronal plane	
16	Run-off Road (2)	Original	200
17		Updated	
18		Coronal plane	

The positioning of the HBM was determined in accordance with a study by Reed et al. [40]. For the passenger positioning, the seat was at mid-height, 3/4 to the rear of the travel range in accordance with what has been reported as a common seating position for passengers [41].

3.5.1 Load Cases

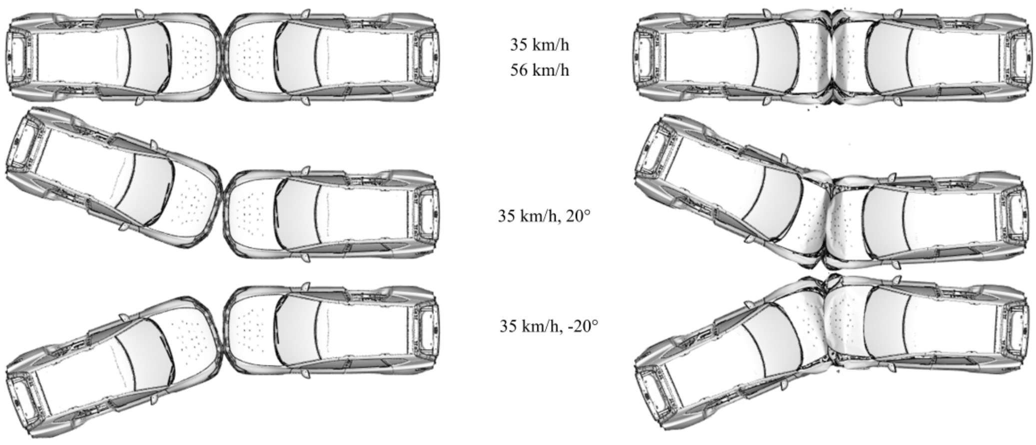

Figure 3.6: Schematic of the simulated frontal impacts. The simulated 6 DoF accelerations and rotations were applied from the car to the right in the figure.

Firstly, a low severity case was simulated, modeling a head on collision with full width overlap (car to car) impact in 35 km/h with a rigid occupant compartment (6 Degrees of Freedom (DoF)), recording translations and rotations in x, y, and z direction, Figure 3.6. As a variation of the 35 km/h impact, it was decided to conduct two different impact cases varying the angle of this impact, Figure 3.6. That created two oblique cases, one with an impact angle of 20° and one with an impact angle of -20°. This introduced a rotation to the impact pulse which gave the opportunity to observe how this affected the loading of the vertebrae. To apply the update in a higher severity impact, a full frontal 56 km/h impact was also simulated.

The run-off road (1) scenario simulated was a run-off road crash referred to as "Ditch" presented by Jakobsson et al. [42], where the car would go off road into a ditch, introducing a roll motion and pitching rotation to the car. In this case, the roll motion contributes to an increased vertical loading of the driver. On the contrary, the run-off road (2) scenario introduces this roll motion to the passenger side of the vehicle model, which instead increases the vertical loading for the passenger.

For all the simulations, intrusions into the occupant compartment were limited and neglected for the occupant compartment simulation by using the rigid compartment model.

3.5.2 Analysis

To investigate whether variations of the spinal curvature influenced the occupant response in other aspects than vertebral fractures, some additional data from the simulations were analyzed. By visually observing the results of the simulations, it was noted whether any submarining occurred, if the feet had contact with the interior of the occupant compartment and whether the torso was subject to any rotation. The loading of the knees was examined by evaluating the magnitude of the force along the femurs, the peak hip displacement was recorded as well as the belt force and pelvis acceleration. The HIC was also noted, although no head rotational metric was used.

Thereafter, the peak forces for each vertebra were analyzed. The force component of most interest was the compressive, negative force component in z direction, since this is the force that contributed to the compressive strain of the vertebrae. Furthermore, the moments in positive y direction were observed, which was due to the forward rotation of the upper body (flexion of the spine), 3.7. The positive and negative moments in x direction were also recorded to examine how the lateral bending of the upper body could affect the loading of the vertebrae. The peak strains were also derived for each vertebra. From these metrics, it could be possible to get an indication of how the risk of fracture would change in the vertebrae after the update. To evaluate the peak strains further, a visual inspection of the fringe plots of the vertebral body top and bottom were executed, which was done to ensure that no single element, or small area, was the main contributor to the max strain value in a larger portion of the simulations.

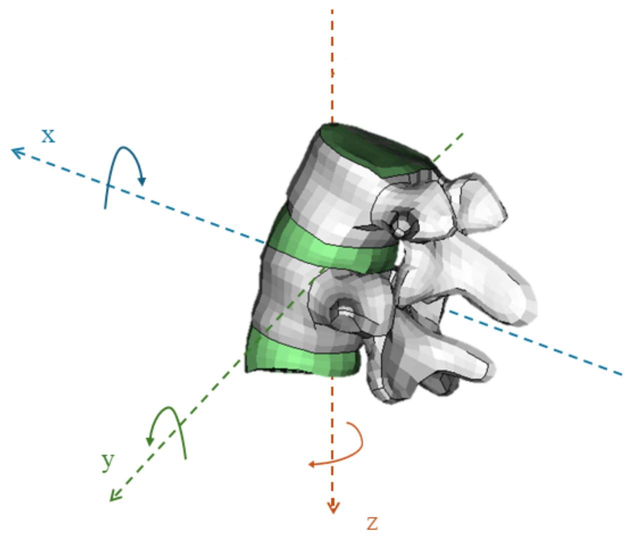

Figure 3.7: A Functional Spine Unit (FSU) with defined coordinate system. Moments in x, y or z direction are displayed as rotations around axes.

3.5.2.1 Extraction of peak strains

It was of interest to study the peak vertebral body trabecular bone inferior-superior strain as part of the analysis of the simulations, since this strain is an injury mechanism for vertebral fractures. This is the strain referred to in this thesis. The strain is presented for all thoracic and lumbar vertebrae, given that their injury mechanism is similar and differ from that of the cervical vertebrae. The loading contributing to these strains were the compressive force of the vertebrae (the negative force component in z direction, Fz-), as well as the moments in x (Mx), y (My+) and to some extent z (Mz) moments. The Injury Assessment Reference Values (IARV) regarding strain were derived using Iraeus et al. tissue-based injury risk function for compression fractures in the lumbar spine, meaning compressive strain in the direction of the local vertical vertebrae body axis, at 50% risk of fracture for a 45 year old male [6]. It was developed using a lumbar spine FE mesh based on an average sized female, with the main direction being the inferior-superior direction. The model was validated through comparison with PMHS physical tests conducted on female and male subjects. To fit the male subjects, the FE model was scaled into one representative of the average male. For the injury risk function, age, sex and level of vertebrae were deemed important characteristics. Finally, the injury risk function was compared by using another PMHS data set to evaluate the feasibility.

3.5.2.2 Linear Regression Model

To determine if there was a relationship between peak strain and the other variables chosen for analysis respectively, linear regression models were created. This was done using the NumPy library *polyfit* and *polyval* functions which together create a regression line minimizing the squared error [43, 44]. Linear regression models were created for peak compressive strain against the peak positive y moment, peak compressive strain against the peak compressive force, as well as peak compressive strain against the peak x moment. The peak x moment was retrieved by comparing the negative and positive peak component and using the one of largest magnitude. To get insight into how well the linear regression models actually model the dependence, the coefficient of determination, R^2, as well as the p-value were retrieved using SciPy's *lingregress* function [45]. This was done for the baseline simulation results versus the updated, as well as baseline versus the coronal plane curvature.

4
Results

In this chapter, the comparison between the SAFER HBM spinal curvature and the predicted 50th percentile model are presented. Thereafter, the updates to the SAFER HBM spinal curvature are accounted for. Finally, the results of the application study, executed in simulations, are presented.

4.1 Comparison of Spinal Curvature

The spinal curvature of the SAFER HBM compared with that of the prediction model by Davidsson et al. [31] was slightly more curved, with some more thoracolumbar lordosis and thoracic kyphosis, Figure 4.1. The vertebrae visualized are C3—L4. For visualization purposes, the curvatures were aligned in vertebra L4. To confirm that the prediction model represented a curvature that an actual 50th percentile male would have, the spinal curvature of one volunteer was also included, Figure 4.1.

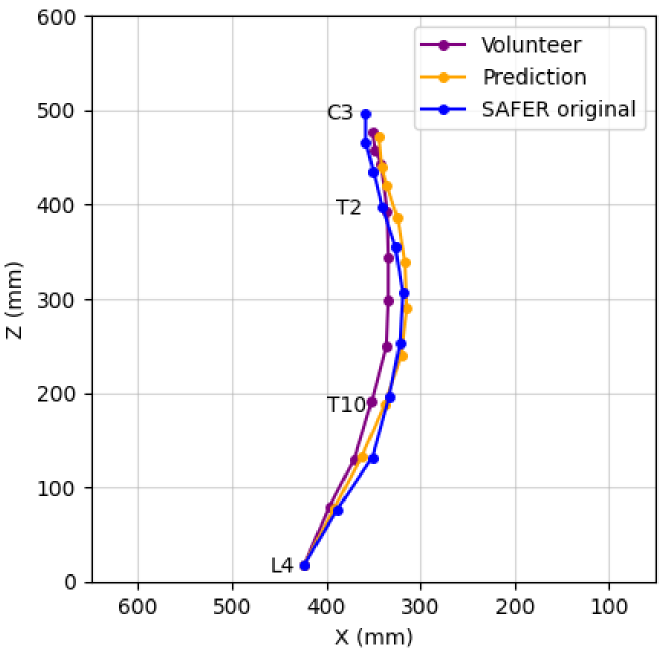

Figure 4.1: The spinal curvature of the prediction model, SAFER HBM original as well as one volunteer (male, 175 cm, 77 kg) extracted from the volunteer study.

4.1.1 Angle Differences

Changes to the spinal curvature were based on the angle differences $\Delta\alpha$ between the SAFER HBM and the prediction model, Table 4.1. The largest difference was observed in vertebra T4, T6, T10 and T12.

Table 4.1: Original angles between vertical line and adjacent vertebra (°), rounded to one decimal.

Vertebra	SAFER	Predicted	$\Delta\alpha$
C5	-0.2	6.0	6.2
C7	14.8	15.6	0.8
T2	13.8	18.2	4.4
T4	18.3	9.4	-8.9
T6	9.3	2.2	-7.1
T8	-3.2	-6.7	-3.5
T10	-11.5	-18.3	-6.8
T12	-15.6	-23.9	-8.3
L2	-33.9	-28.0	5.9
L4	-31.0	-28.0	3.0

4.2 Updating the Curvature

The spinal curvature update of the SAFER HBM was executed as described in Chapter 3. After articulation, it was found that the largest difference was observed in T2, L2 and L4, Table 4.2. The vertebral laminae locations before and after updating the spinal curvature can be found in Appendix H.

Table 4.2: Angles between vertical line and adjacent vertebra (°) for the target spinal curvature, rounded to one decimal.

Vertebrae	SAFER updated	Predicted	$\Delta\alpha$
C5	6.0	6.0	0.0
C7	15.5	15.6	0.1
T2	18.6	18.2	-0.4
T4	9.3	9.4	0.1
T6	2.3	2.2	-0.1
T8	-6.7	-6.7	0.0
T10	-18.3	-18.3	0.0
T12	-23.9	-23.9	0.0
L2	-27.7	-28.0	-0.3
L4	-28.3	-28.0	0.3

When inserting the kinetic position into the Marionette tool, it was discovered that a contact arose between vertebra T12 and L1. This limited the range of possible rotation for these vertebrae and resulted in an inability to achieve the targeted spinal position. To avoid contact between the vertebrae in the updated SAFER HBM, the inferior articular processes of T12 were angled slightly posteriorly by local direct form morphing (4 mm). Doing this, the reference node that had been utilized to extract the vertebra position was moved and could no longer be used as a reference. Therefore, a new node was selected that was closer to the original location to not create confusion when analyzing the results. After simulating the HBM into position, the angle difference $\Delta\alpha$ differed slightly from the target position. Finally, after implementing the spinal curvature, the largest angle difference was observed in T6 and T12, which was in the locations where the original curvature deviated the most from the prediction model (T4, T6 as well as T10 and T12), Table 4.3.

Table 4.3: Resulting angles between vertical line and adjacent vertebra (°), rounded to one decimal.

Vertebrae	Actual SAFER updated	Predicted	$\Delta\alpha$
C5	6.0	6.0	0.0
C7	15.7	15.6	-0.1
T2	18.2	18.2	0.0
T4	9.3	9.4	0.1
T6	2.5	2.2	-0.3
T8	-6.9	-6.7	0.2
T10	-18.5	-18.3	0.2
T12	-23.3	-23.9	-0.6
L2	-28.0	-28.0	-0.0
L4	-28.2	-28.0	0.2

After $\Delta\alpha$ between the prediction model and the original, target and updated SAFER spinal curvature was derived, Figure 4.2, it was seen that the angle difference was reduced substantially with the updates. Yet, the updated model did not equal the target model entirely.

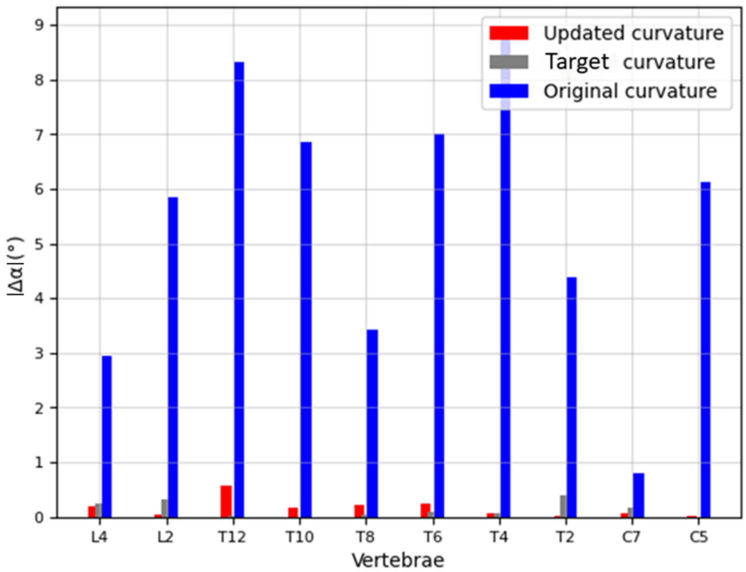

Figure 4.2: The absolute angle differences, $|\Delta\alpha|$, of the spinal curvature between the SAFER HBM and the prediction model.

The prediction model had less lordosis in the upper thoracic region. It was seen that the updated spinal curvature, in red, was of a straighter posture in this area as compared to the original curvature, in blue, Figure 4.3.

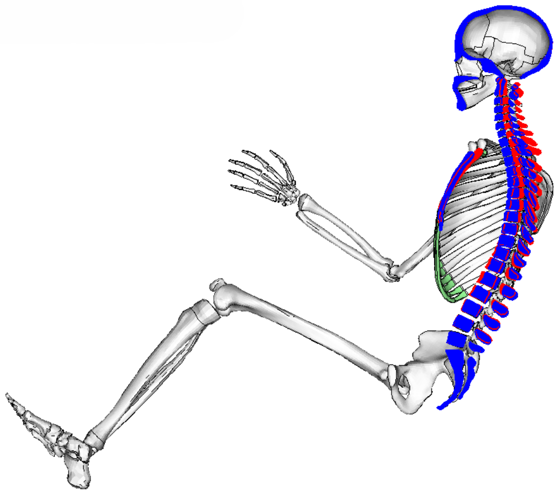

Figure 4.3: The skeleton of the SAFER HBM, with the updated SAFER HBM spine (red) and the original spinal curvature of the SAFER HBM (blue).

By visualizing the lamina lines (aligned in L4) of the original and updated SAFER model as well as the prediction model, Figure 4.4, it was observed that the updated SAFER HBM spinal curvature was closer to the posture of the prediction model than the original SAFER curvature. The largest remaining difference was, as mentioned, still observed in the thoracic spine.

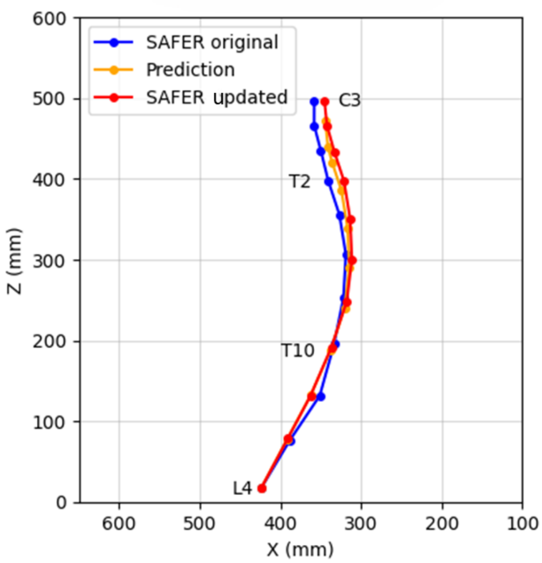

Figure 4.4: The spinal curvature of the original and updated SAFER HBM (lamina line), as well as the prediction model of the 50th percentile male.

4.2.1 Application Study

In the following subsections, a portion of the results from the application study are presented for all impacts cases, with paired simulations for the original SAFER HBM and the SAFER HBM with an updated spinal curvature. Initial posture of the occupants were the same for all impact scenarios, Figure 4.5.

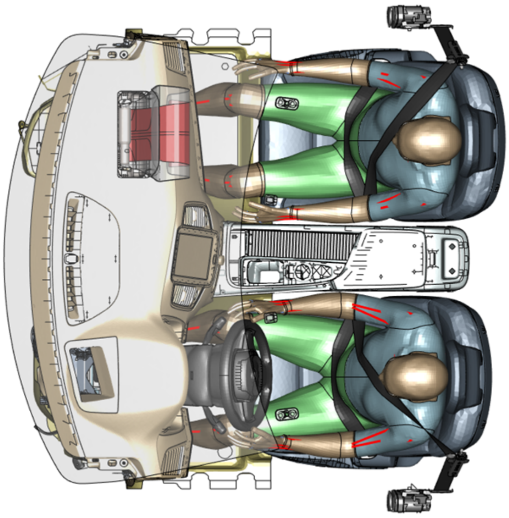

Figure 4.5: Initial position of the occupants during simulation.

4.2.1.1 Frontal Impacts

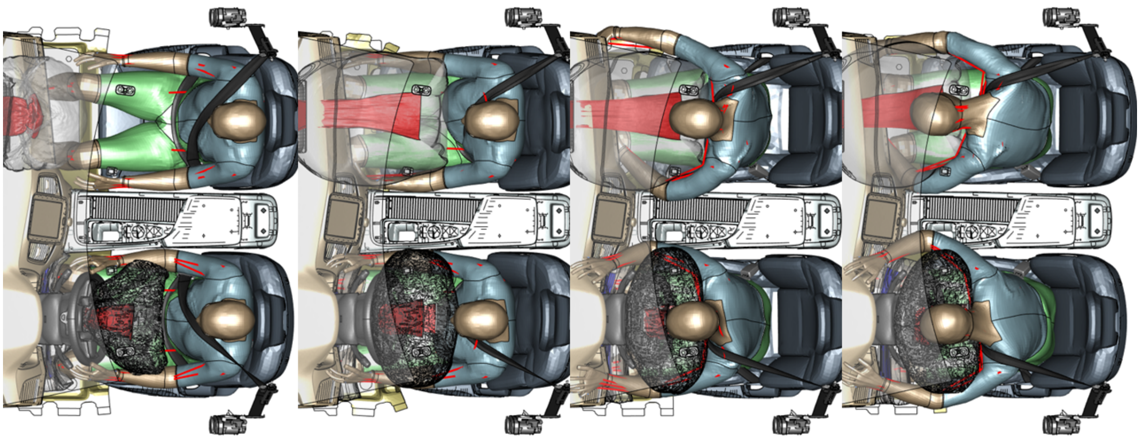

Figure 4.6: Kinematics of the occupants at time 30, 60, 90 and 120 ms, frontal impact 35 km/h.

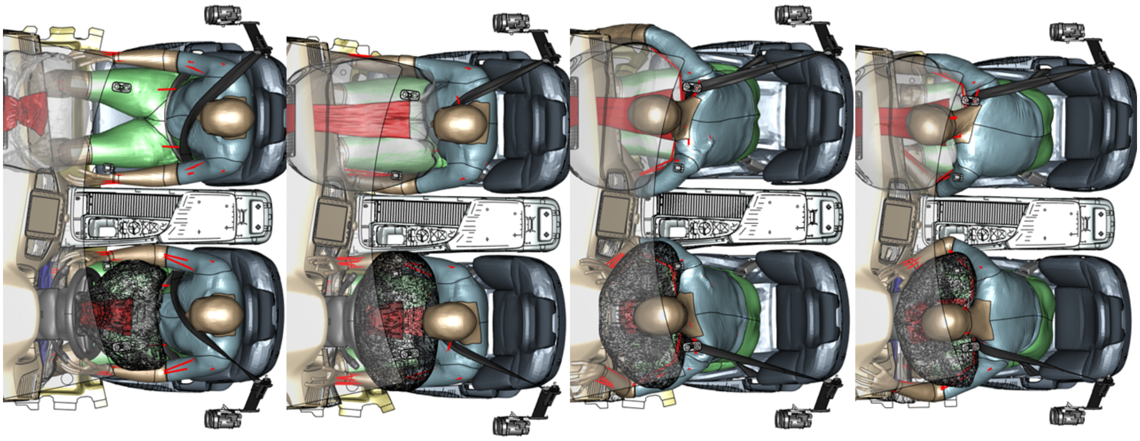

Figure 4.7: Kinematics of the occupants at time 30, 60, 90 and 120 ms, frontal impact 56 km/h.

Both a low severity, 35 km/h, and a high severity, 56 km/h, frontal impact was simulated, Figures 4.6, 4.7. For both these cases, the peak compressive strain on the vertebrae for the baseline spinal curvature as compared to the updated spinal curvature simulation were similar, with small deviations, Figure 4.8. There were larger deviations for the higher severity case, mainly for the passenger in the region between vertebra T7 to T11. For both these impact scenarios, the global peak strain was located in vertebra L5 for the passenger position. The strains were well below the 50% IARV for vertebral body fracture.

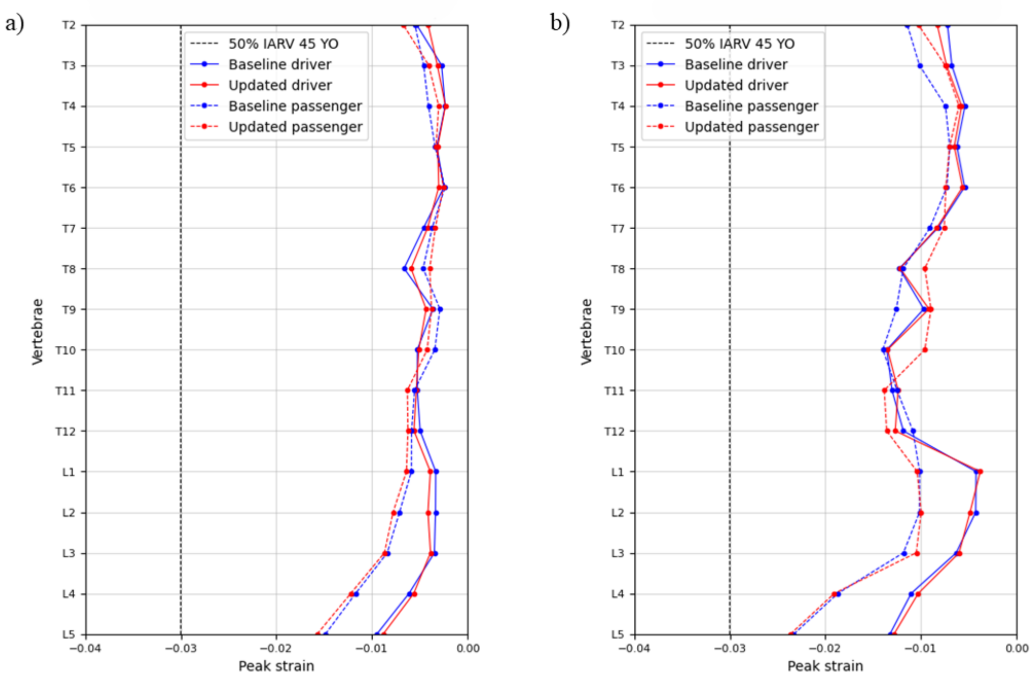

Figure 4.8: Peak vertebral strain, full frontal a) 35 km/h, b) 56 km/h.

4.2.1.2 Oblique Impacts

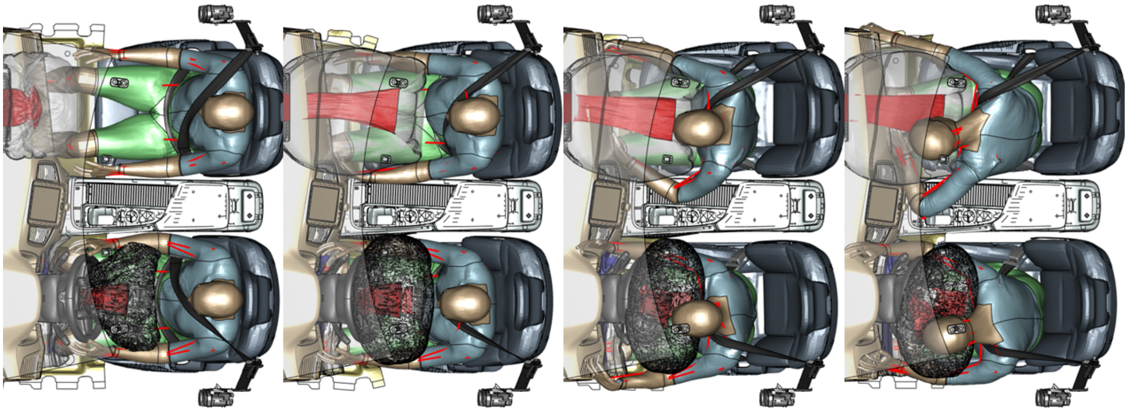

Figure 4.9: Kinematics of the occupants at time 30, 60, 90 and 120 ms, oblique impact 35 km/h (-20°).

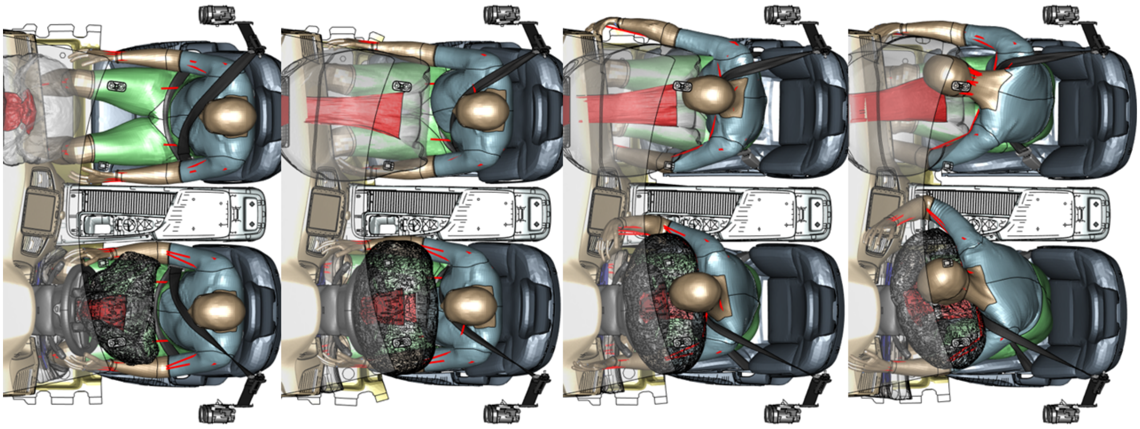

Figure 4.10: Kinematics of the occupants at time 30, 60, 90 and 120 ms, oblique impact 35 km/h (20°).

As presented, two oblique cases were created by varying the low severity, 35 km/h, frontal impact with impact angle of ±20°, Figures 4.9, 4.10. As for the full frontal impacts, the spinal curvature update did not seem to generate any drastic differences with regards to the vertebral strain, Figure 4.11, only small deviations between the baseline and updated. The differences were larger for the impact with a positive impact angle, but the magnitude was still realtively low.

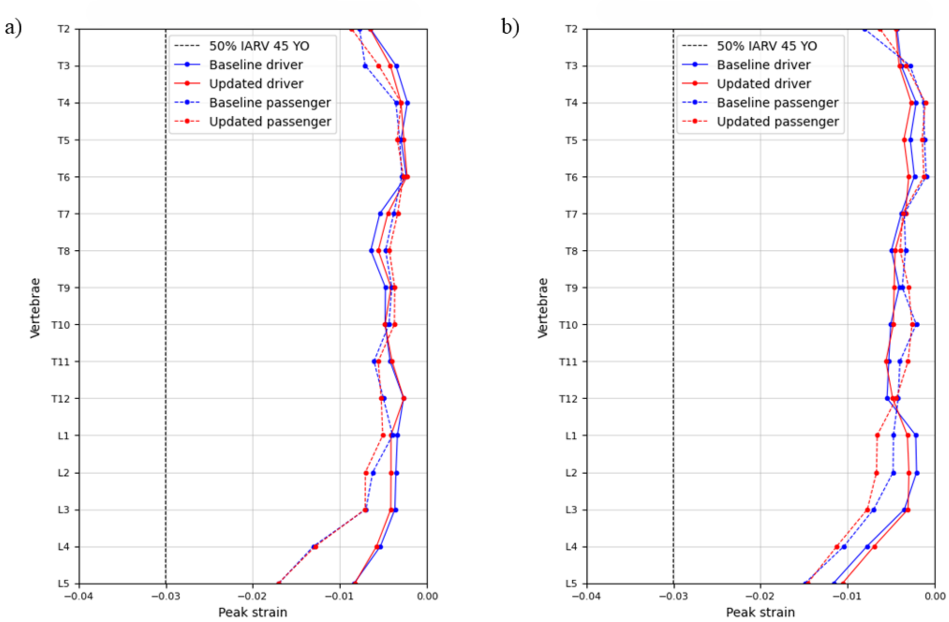

Figure 4.11: Peak vertebral strain, frontal 35 km/h a) (-20°), b) (20°).

4.2.1.3 Run-Off Road (1)

Finally, two run-off road scenarios into ditches were simulated. In these two cases, the peak compressive force was one parameter of interest, since the negative component in z direction was hypothesized to be prominent for these cases.

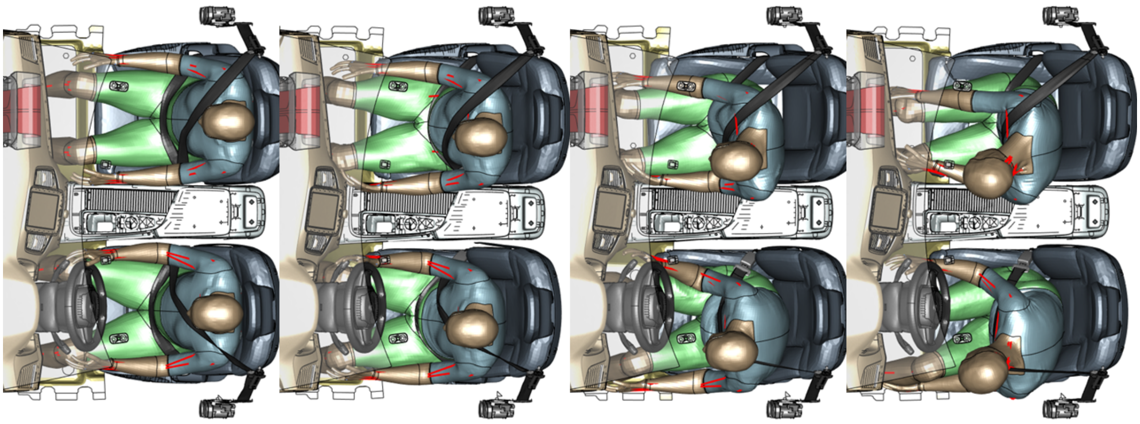

Figure 4.12: Kinematics of the occupants at time 30, 60, 90 and 120 ms, run-off road (1).

Run-off road (1), Figure 4.12, introduced a roll motion, which meant that the driver was expected to be subject to a larger compressive force, which was confirmed by studying the peak compressive force, Figure 4.13. The driver experienced larger compressive peak force as compared to the passenger in both the baseline and updated simulation. The differences between baseline and updated were the most prominent for the driver, and the peak forces were of largest magnitude in the lumbar spine.

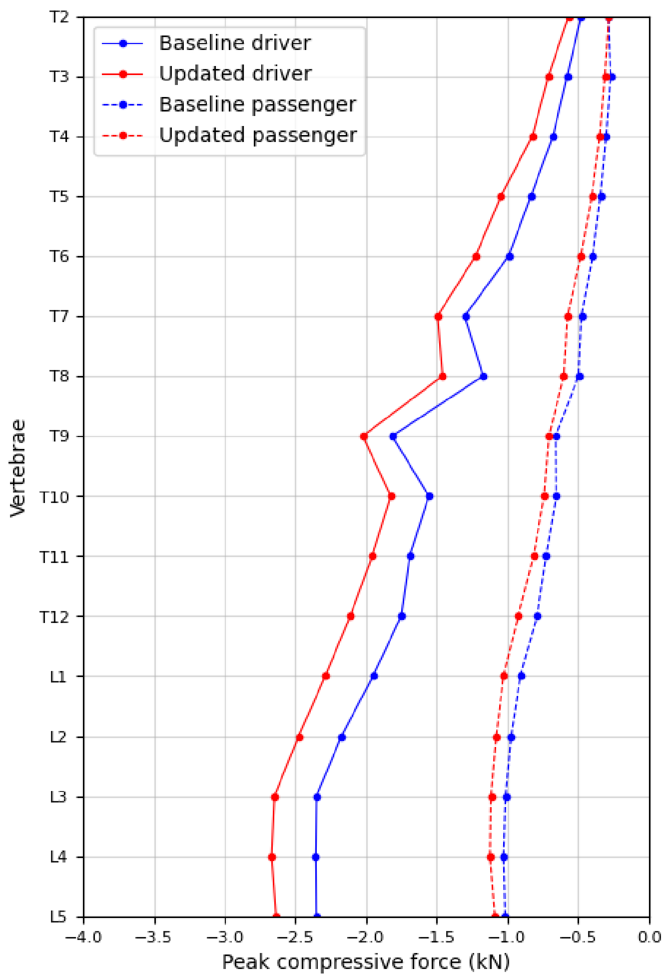

Figure 4.13: Peak vertebral compressive force, run-off road (1).

The peak compressive strain had the largest magnitude in vertebra L5 for the driver, Figure 4.14, which corresponds to the global maximum of the peak y moment (flexion) for the updated simulation, which also appear in vertebra L5. For the baseline however, the y moment is larger (vs. updated) and occur in L1, which corresponds to the location of one of the peak strains for the baseline case. The global peak strain of the baseline driver is likely due to the peak force being at L5 level, Figure 4.13.

Regarding the driver, it seemed as if the strains and y moments were increased with the updated spinal curvature in the region of T2—T10, and L4—L5, whilst they were decreased between vertebra T11—L3.

For the passenger, the deviations were not as prominent, but the same pattern regarding y moment and compressive strain seemed to be consistent.

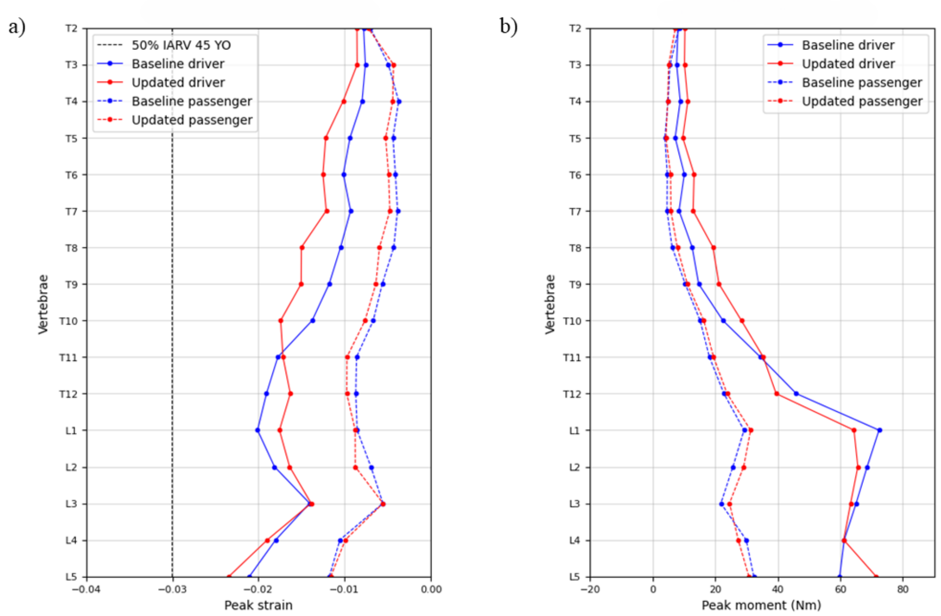

Figure 4.14: a) Peak vertebral strain, run-off road (1). b) Peak y moment, run-off road (1).

4.2.1.4 Run-Off Road (2)

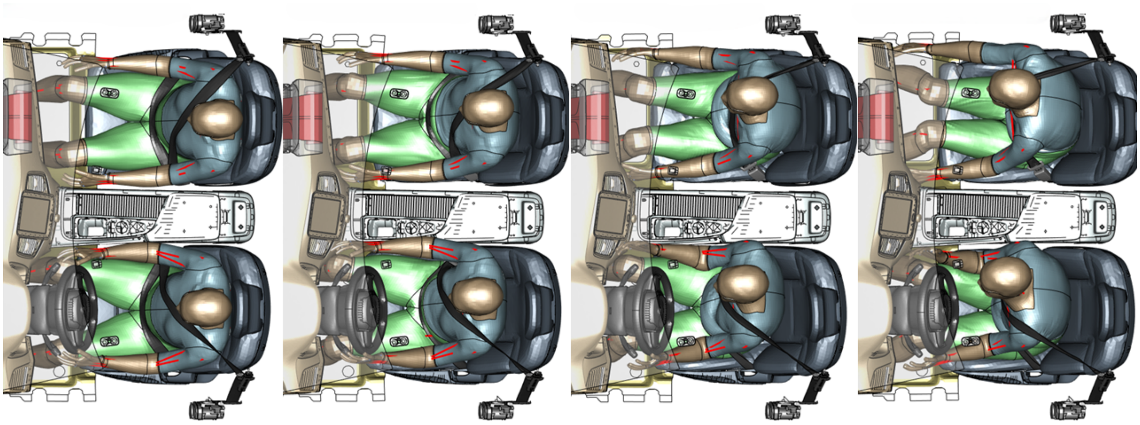

Figure 4.15: Kinematics of the occupants at time 30, 60, 90 and 120 ms, run-off road (2).

In the run-off road (2) scenario, Figure 4.15, the roll motion mainly affected the passenger instead. This implied that the peak compressive force should have been of higher magnitude for the passenger rather than for the driver. This hypothesis was confirmed, Figure 4.16. As for run-off road (1), the peak forces were of larger magnitude for the updated spinal curvature in comparison to the baseline.

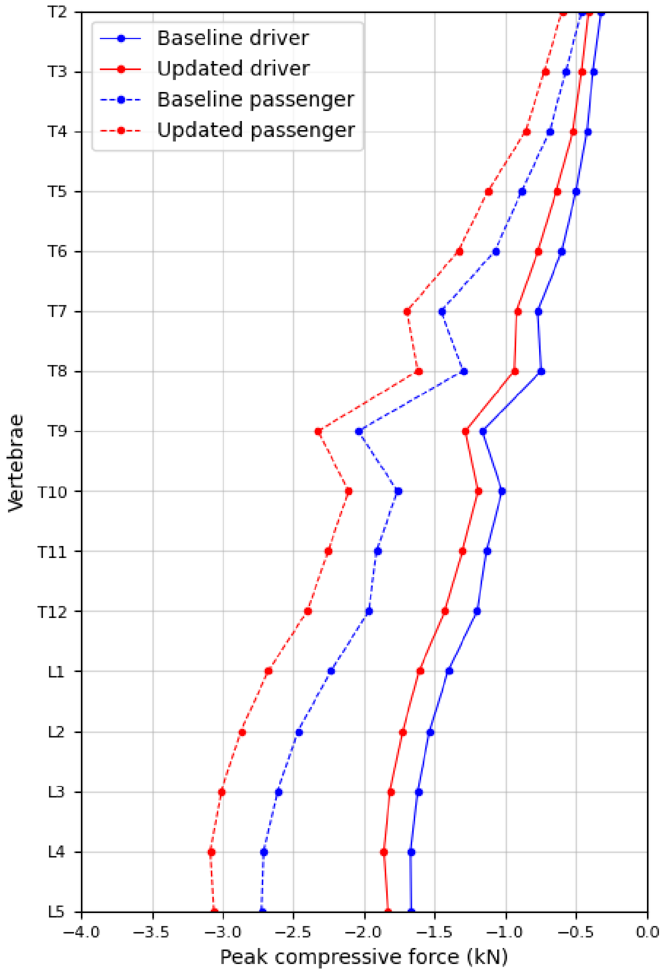

Figure 4.16: Peak vertebral compressive force, run-off road (2).

For the peak vertebral strain, it was expected to find the same pattern as in run-off road (1), which was confirmed, Figure 4.17. The peak strain was of largest magnitude in L5 for the updated curvature simulation, but in vertebra T12/L1 for the baseline (both in the passenger position). The peak strain seems to have increased with the updated spinal curvature in region T2—T10, L3—L5 whilst it decreased with the updates between vertebrae T11—L2, both for the driver and passenger position. As expected, the peak y moment was thus larger for the updated simulation in the regions that experienced larger peak strain with the updates (T2—T10 and L3—L5).

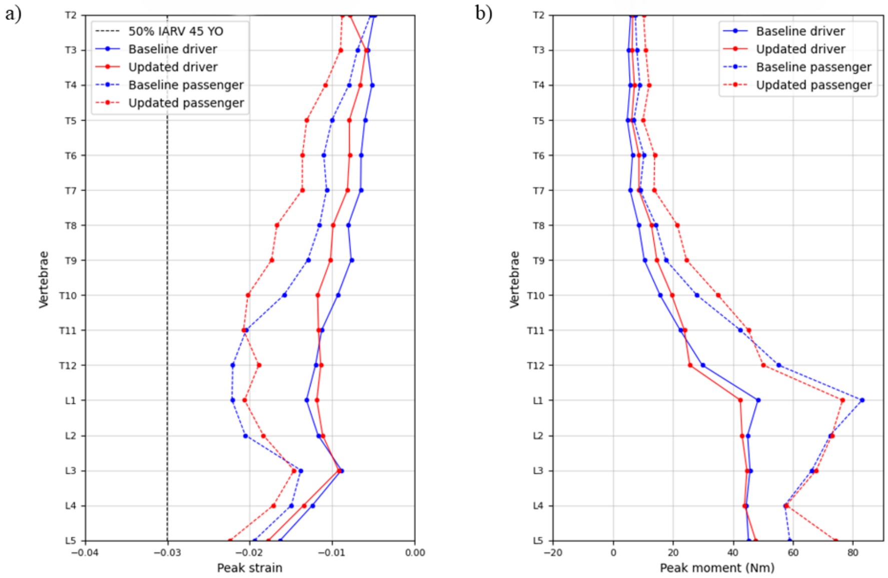

Figure 4.17: a) Peak vertebral strain, run-off road (2). b) Peak y moment, run-off road (2).

4.3 Coronal Plane Curvature Update

The aim was to vary the Cobb angle in the coronal plane by 9°. After simulating this position of the spine into place, the resulting actual Cobb angle was approximately 7°. It was decided that the magnitude of this coronal curvature was enough for the cause of studying how the strain of the vertebrae could be affected by curvature in the coronal plane, while still below the threshold of 10°.

After applying the variations to the spinal curvature in the coronal plane, the HBM and its spine acquired a right curved posture as compared to the original position, Figure 4.18.

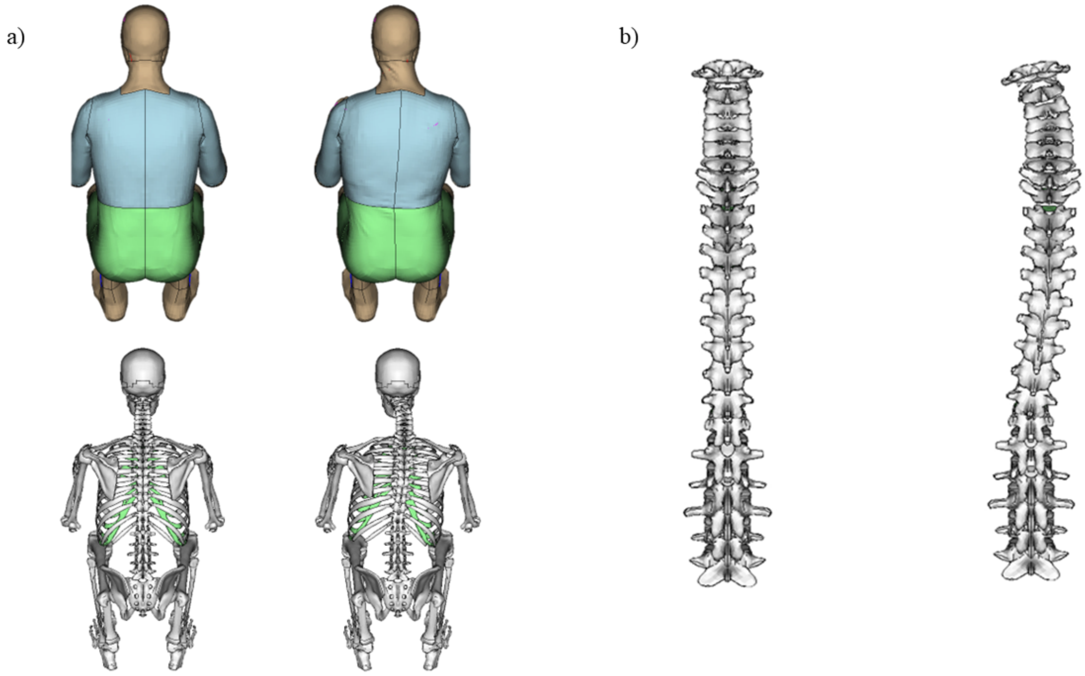

Figure 4.18: a) Full body comparison of the straight spine as compared to the spine with a curvature in the coronal plane. b) Spinal column comparison of the straight spine as compared to the spine with a curvature in the coronal plane.

4.3.1 Application Study

After applying the variations to the spinal curvature in the coronal plane, the changes were applied in simulation. In this section, the result from all load cases are presented.

4.3.1.1 Frontal Impacts

The peak strain for the driver was of higher magnitude for the coronal curvature case between vertebra T2 and T9, whilst being lower between vertebra T9 and L1 and approximately the same in the lumbar spine, Figure 4.19. For the passenger, the peak strains were higher for the coronal curvature simulation in most regions, with exceptions in vertebrae T4 and T8. Studying the peak strain of the higher severity frontal impact, there was not a distinct pattern of differences between the cases for the driver. For the passenger, the peak strain was larger for the coronal curvature case in most regions, but similar to the baseline case in some, namely T4, T6, T9, T10 and L5. For both positions and curvatures, the peak strains were well below the 50% IARV, but of highest magnitude in vertebra L5, which is an observation that could be done for the lower severity case as well.

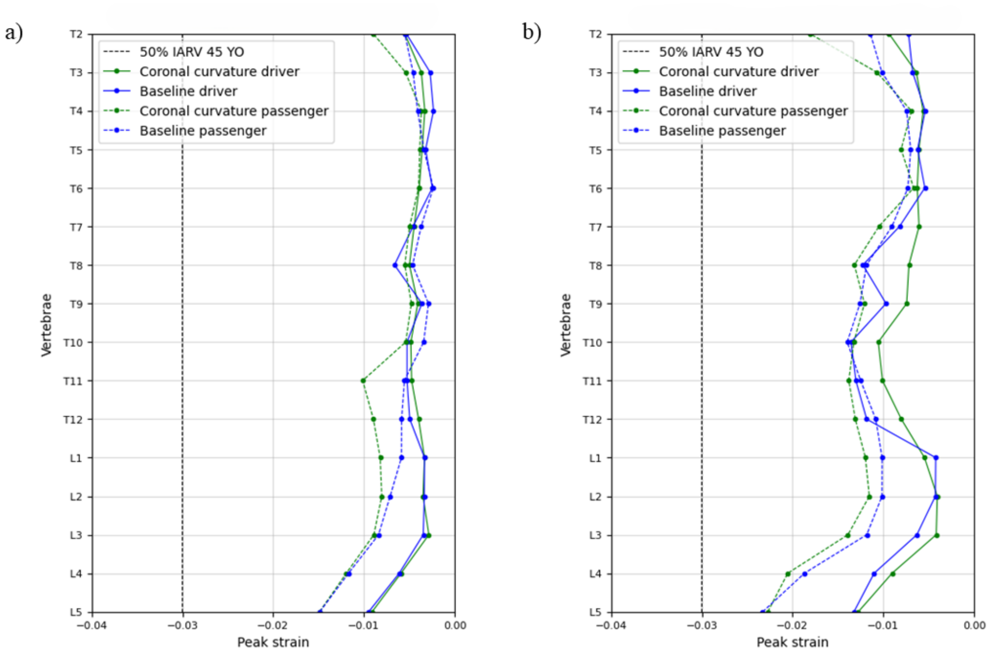

Figure 4.19: Peak vertebral strain, full frontal a) 35 km/h, b) 56 km/h.

4.3.1.2 Oblique Impacts

The low severity frontal impact was simulated with varying impact angles, ±20°, resulting in two oblique impacts. Regarding the peak vertebral strain in the scenario with a negative impact angle, the passenger seemed to be subject to roughly the same vertebral strains for both the baseline case and the case with coronal curvature, with slight variations in some vertebrae, Figure 4.20. For the driver, the variations were larger and most prominent in vertebra T7, T8 and T9. However, in most areas, the strains were of smaller magnitude for the coronal curvature case as compared to the baseline.

For the passenger in the positive impact angle scenario, the strain was of higher magnitude in both the thoracic and lumbar spine for the case with a coronal curvature.

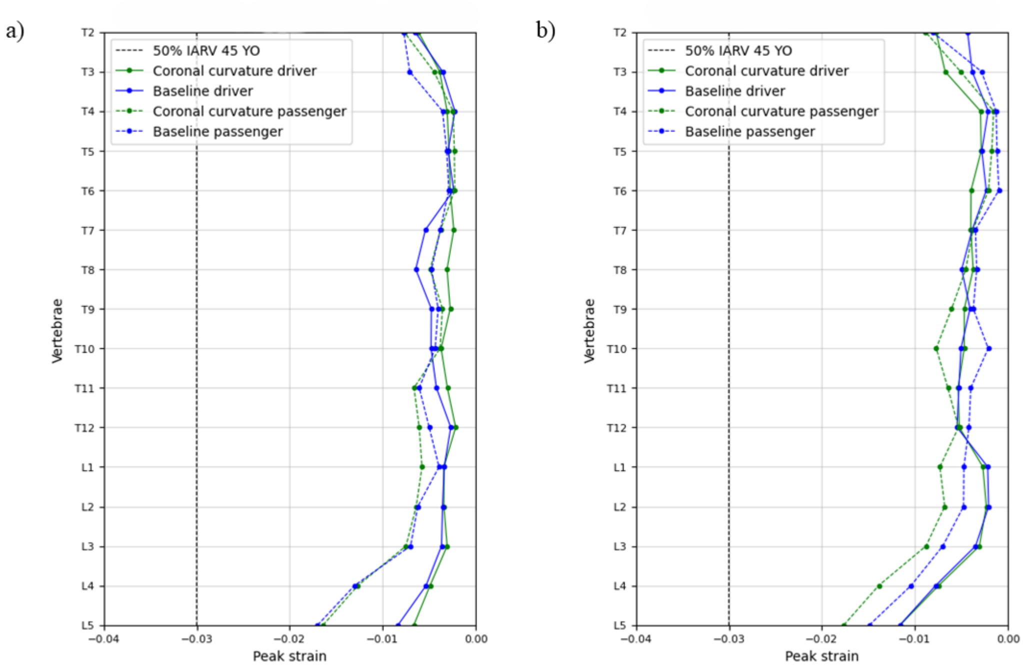

Figure 4.20: Peak vertebral strain, oblique impact 35 km/h a) (-20°), b) (20°).

4.3.1.3 Run-Off Road

For run-off road (1), Figure 4.21, it was seen that the peak force in the vertebrae was increased with the coronal curvature case for both positions, with an exception in T7 for the driver. For both positions, the peak force was largest in the lumbar region, L5 for the driver and L3 for the passenger.

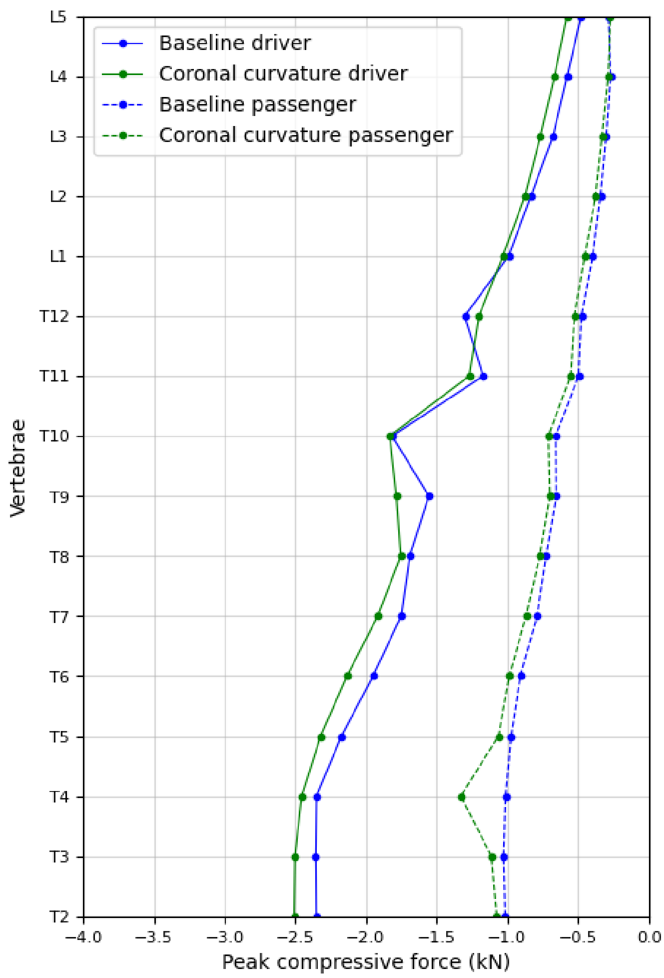

Figure 4.21: Peak compressive force, run-off road (1).

For the driver, the peak y moment was of higher magnitude in vertebrae T2—T9 as well as L5 for the case with the coronal curvature, Figure 4.22. It was approximately the same in vertebra T10 and L4, but lower in vertebrae T11—L3. For the passenger, the deviations were smaller than those of the driver. The magnitudes were similar in the region between vertebrae T2—L1, but larger for the baseline case in the rest of the lumbar spine.

The peak strain was the largest for the driver in vertebra L5, still below the 50% IARV. Generally, the strain seemed to somewhat increase with the updates, but there were exceptions in some vertebra, e.g. in vertebra T10.

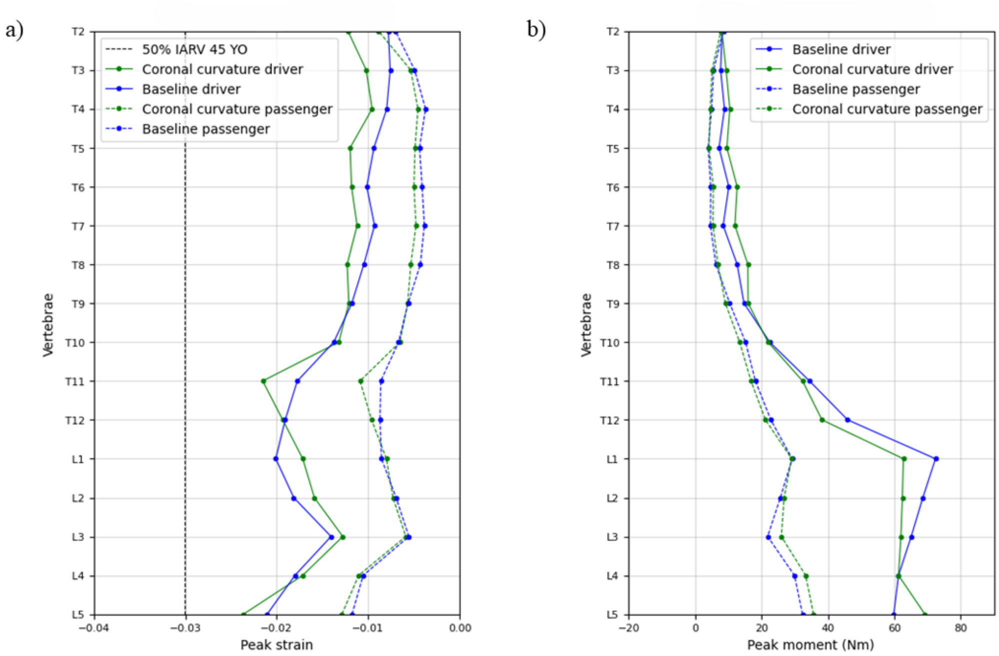

Figure 4.22: a) Peak vertebral strain, run-off road (1). b) Peak y moment, run-off road (1).

For run-off road (2), the passenger was subject to larger compressive forces than the driver, as was expected given the scenario. As for run-off road (1), the force was increased with the coronal curvature for both positions. It can be noted that the global maximum peak force was in L5 with a magnitude of approximately 2.8—2.9 kN as compared to the maximum of 2.5 kN in run-off road (1), which would imply a more aggressive loading scenario, Figure 4.23.

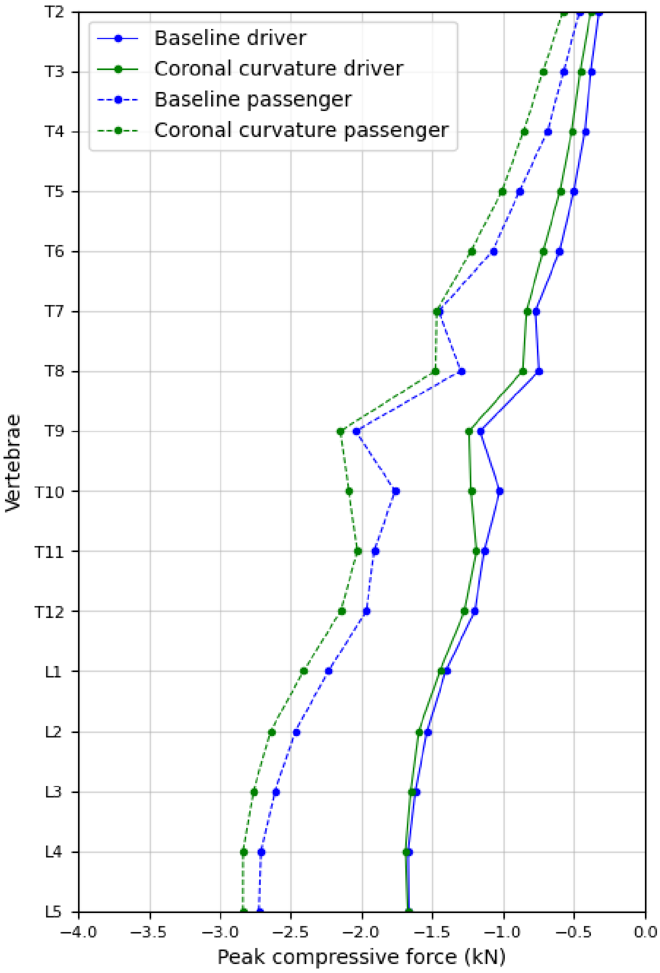

Figure 4.23: Peak compressive force, run-off road (2).

For the peak y moment, the trend was again opposite as compared to run-off road (1), since the moments were of higher magnitude for the passenger than for the driver. The driver experienced similar peak moments in the baseline and coronal curvature case, but there were variations regarding the passenger, e.g. an increase in moment in vertebra L5, Figure 4.24. The peak strain was, unlike the first run-off road case, located in vertebra T12 for the passenger, and of larger magnitude for the baseline simulation. In the upper thoracic region (until vertebra T9) the strain was larger with the coronal curvature case, as well in the lower lumbar region. This trend was similar between driver and passenger.

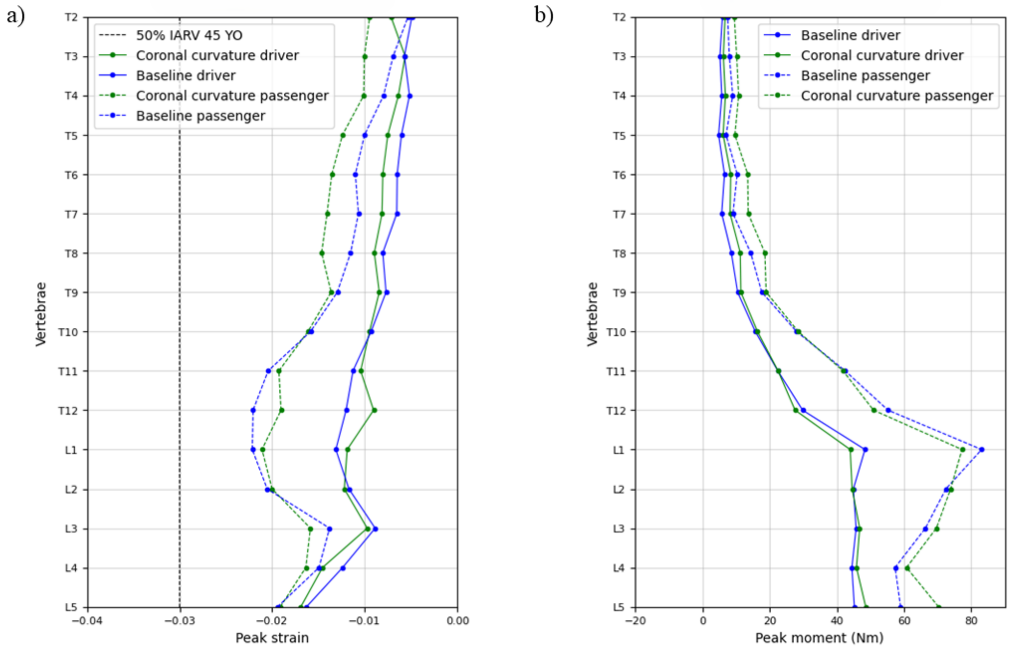

Figure 4.24: a) Peak vertebral strain, run-off road (2). b) Peak y moment, run-off road (2).

4.4 FE Model Quality

It was observed that the FE model quality in terms of AR, Element Jacobian, warping and skewness deviated less than one percentage point from the original quality in all measures across all elements, Appendix D. The element with maximum deviation from the optimum could in some instances be found in related areas to the spine, Table 4.4, 4.5, 4.6, 4.7, and 4.8.

Table 4.4: Shell elements with maximum warping.

	Part ID	Value
Original	Thorax T4 Vertebra Cortical Bone	19.96
Updated	Neck Soft Tissues Inner Null Left	36.11
Coronal plane	Neck Soft Tissues Inner Null Left	38.76

Table 4.5: Shell elements with maximum skewness.

	Part ID	Value
Original	Abdomen L5 Vertebra Cortical Posterior	59.88
Updated	Thorax T12 Vertebra Cortical Posterior	66.98
Coronal plane	Thorax T2 Vertebra Cortical Posterior	62.40

Table 4.6: Solid elements with minimum Element Jacobian.

	Part ID	Value
Original	Abdomen Pelvis Innominate Trabecular Left	0.32
Updated	Thorax Spine to Internal Organs attachment	0.25
Coronal plane	Thorax Spine to Internal Organs attachment	0.23

Table 4.7: Solid elements with maximum warping.

	Part ID	Value
Original	Thorax Rib Intercostal Muscle External	20.00
Updated	Neck Soft Tissues	36.11
Coronal plane	Abdomen Hip Fat Left	40.04

Table 4.8: Solid elements with maximum skewness.

	Part ID	Value
Original	Lower Extremity Femur Trabecular Left	60.00
Updated	Thorax T12 Vertebra Trabecular Bone Posterior	66.98
Coronal plane	Thorax Rib Intercostal Muscle Inner	71.31

4.5 Linear Regression Models

To investigate if there was a dependence between strain and the other variables chosen for analysis after the application study, linear regression models were created for three vertebrae, using data from all crash simulations. In this section the linear regression results based on the sagittal spinal curvature update is presented, the linear regression models were also created for the same variables for the coronal curvature and are presented in Appendix E.

In these plots, the red colored lines and markers represent the data from the simulations using the updated spinal curvature, as before. The blue colored lines and markers represent data from the baseline simulations. To distinguish between the data from the driver and the passenger, driver is marked with dots and passenger are represented by the star markers. The R^2 and p-values has been rounded to two decimals.

The peak strains and peak moments were extracted independent of time, for each vertebra in each simulation. The results from the regression models implied that the relationship between strain and positive y moment was linear for vertebra T6, as $R^2 = 0.99$, supported by $p < 0.05$, Figure 4.25 for both the baseline and updated results. The same applies for the compressive force, $Fz-$. As for the peak strain and x moment, no statistically significant relationship could be proven with these results, given $p > 0.05$.

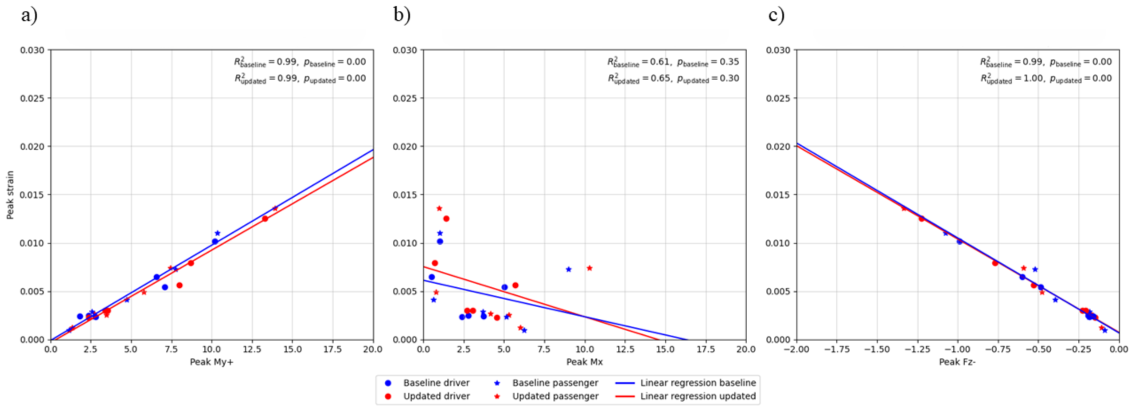

Figure 4.25: The linear regression between strain and a) y moment, b) x moment, c) compressive force for vertebra T6.

For vertebra L1, a strong linear relationship was observed between the strain and y moment, both for the baseline and updated results, with a slightly higher R^2 for the updated simulation results (0.99 as compared to 0.98) Figure 4.26. This relationship was deemed significant, $p < 0.05$. A larger spread of the data points was observed for the compressive force, but a linear relationship was still found. Regarding the relationship between the strain and x moment, similarly to the results for vertebra T6, there was no significant relationship supported by the results of vertebra L1 given $p > 0.05$.

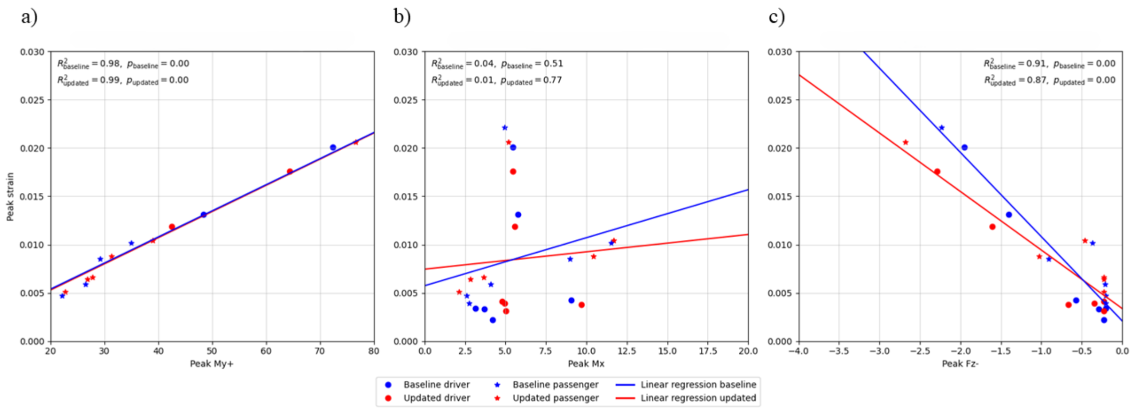

Figure 4.26: The linear regression between strain and a) y moment, b) x moment, c) compressive force for vertebra L1.

The results for vertebra L5 deviated slightly from those for vertebra T6 and L1. Like the previous results, there was also a significant relationship found between the strain and y moment for vertebra L5, p-value< 0.05, Figure 4.27. R^2 for this case (0.33 and 0.55) was however lower as compared to the models previously presented.

Regarding the relationship between strain and compressive force, it was observed that the baseline results did not support a significant linear relationship between the variables, $p > 0.05$. The updated results did on the other hand present a linear relationship that was significant, $p < 0.05$, but note that $R^2 = 0.38$, which is relatively low.

For strain against x moment, a possible linear relationship could be observed for both the baseline and updated case, $p < 0.05$. As for the relationship between strain and compressive force, it seemed to be a stronger linear relationship for the updated case (with regards to a lower p-value and higher R^2 value).

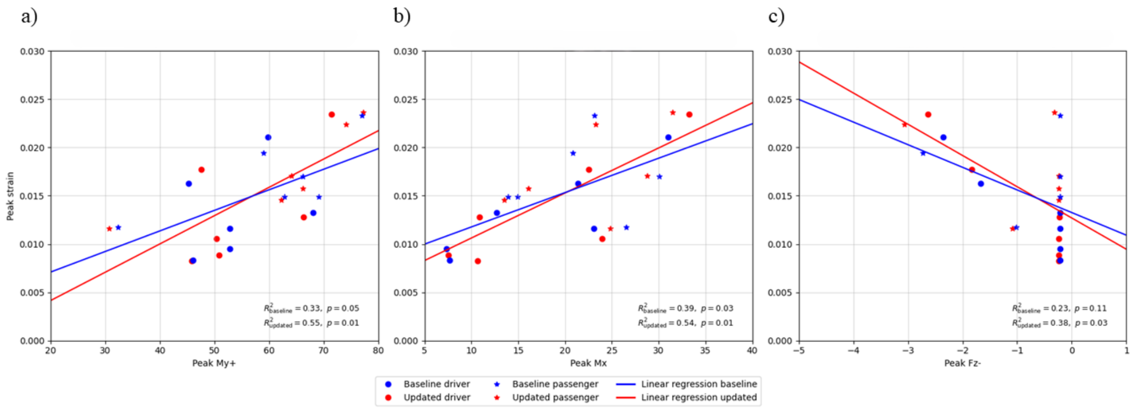

Figure 4.27: The linear regression between strain and a) y moment, b) x moment, c) compressive force for vertebra L5.

5

Discussion

In this thesis, the spinal curvature of the SAFER HBM was updated to match that of a prediction model by Davidsson et al. based on seated volunteers [31]. It was challenging to exactly match the prediction model curvature for the L2—T12 segment due to contact of the inferior articular processes, which is why some minor local geometry updates were also applied using morphing. In comparison with an individual volunteer curvature it was found that the prediction model was plausible, which supported the update of the SAFER HBM curvature. The prediction model as well as the original SAFER HBM spinal curvature were compared to additional models as a way of validation and evaluation. When applying the changes to the spinal curvature of the SAFER HBM, the model quality did not differ much from the original model quality.

The two variations of spinal curvature evaluated in the application study were an updated curvature in the sagittal plane, and an additional model with curvature introduced in both the sagittal plane and the coronal plane. These curvatures were applied in simulations of six different crash scenarios; two frontal, two oblique and two run-off road scenarios. In most cases, the peak force and strain was found in the L5 vertebra, which was hypothesized to be due to factors such as the larger amount of body mass the caudal vertebrae carries as compared to the cranial vertebrae. As seen in Table G.1 in Appendix G, vertebra L5 was also the vertebra that absorbed the most amount of energy, which was assumed to be partially due to superior-inferior compressive force.

The curvature of the spine seemed to have an influence on the level of strain of the vertebrae, which in turn would affect the fracture risk. The most common area of fractures to the thoracolumbar spine is in the interface between the thoracic and lumbar spine, i.e., T12 and L1 with adjacent vertebrae [5]. Because of this injury prevalence, these sites were important to include in the analysis. The hypothesis of this being an area prone to injury was supported by the level of strain in T12/L1 of the passenger in the baseline run-off road (2) scenario.

When the curvature was altered, while treating all bones as rigid, the intervertebral discs were deformed to allow the spine to move into the target position. The initial deformations of the discs could possibly have had an effect on the ability to withstand load, given that this is one of the functionalities of the intervertebral discs. Since the discs were in a deformed state initially in the simulation, it could have reduced their potential of absorbing load and thus possibly increased the loading of the vertebrae. This was assumed to mainly affect the impact scenarios with considerable accelerations in z direction, namely the run-off road cases.

5.1 Volunteer Data

One possible limitation of the thesis was the methodology used in the data collection. The data was collected by measurements via the skin and through ultrasound measurements of the spine. This could be seen as a limitation due to the uncertainty of the measured distances. By using other imaging techniques, e.g. x-ray or MRI, the distances could have been measured more precisely. However, x-ray has the disadvantage of delivering dose to the patient, while MRI cannot be combined with ferro-magnetic metal components commonly used in car seats. The ultrasound device does however introduce an uncertainty, since it is possible that the ultrasonic waves were reflected off another vertebra than the target vertebra. This could occur when imaging the spine, due to e.g. the flexion/extension of the cervical vertebrae or protraction/retraction of the scapulae.

Descriptive data of the volunteers that the model was based on were presented in Table 3.1. There was approximately the same amount of women and men, indicating that the model should describe the curvature of the male and female spine equally well. The age distribution was 16—66 years, which raises the question if it would be representable for an older population. It has previously been stated that the kyphosis of the thoracic spine increase with increased age [46], which could affect the distribution of the loading.

Regarding the weight, the lightest volunteer was approximately the same weight as the 5th percentile female ATD (50 kg and 49 kg respectively), while the heaviest volunteer was approximately the same weight as the 95th percentile male ATD (105 kg and 102 kg respectively). This indicated that the Davidsson et al. prediction model should have the ability to model the spinal curvature for these edge cases. However, the stature of the volunteers did not cover the stature of the 5th percentile female, since the shortest volunteer was 6.5 cm taller than the 5th percentile female ATD. This could have an impact on the stature of the spine, which might influence the curvature. This is one aspect that future research could investigate further.

There was a volunteer with comparable weight and stature to the 50th percentile male, which enabled an analysis of the model's plausibility, Figure 4.1. Here, the characteristics of the curvatures were similar, but the prediction had a more pronounced kyphosis in the thoracic spine. This was deemed reasonable, taking into account that the model should have a certain generalizability, and should therefore not exactly mimic one specimen from the population of the volunteer study.

5.2 Comparison of Spinal Curvature

When comparing the lamina line of the original SAFER HBM spine and the corresponding predicted curvature, as seen in Figure 4.1, it was noted that the SAFER spinal curvature visually appears to be slightly more kyphotic in the thoracolumbar spine, while the predicted curvature was straighter. It could also be seen that the SAFER HBM curvature was of slightly more lordotic nature in the upper thoracic spine. Concluded, the posture of the prediction model was straighter than the original SAFER HBM. Table 4.1 demonstrates the difference in angles numerically in the extracted vertebra locations. It could be observed that the largest angle difference was in T4, while the smallest difference was observed in C7.

To be able to compare the prediction and the SAFER HBM, the methodology of measurements presented by Davidsson et al. was applied when extracting vertebral locations from the SAFER HBM spine. However, the width of some of the vertebrae in the SAFER HBM was not sufficient to measure at the corresponding locations as in the volunteer study [31]. The solution to this was to extract nodes as far out laterally on the lamina as possible, Figure 3.3. This introduced some uncertainty to the curvature, but was however not seen as a limitation since there was already some uncertainty related to the ultrasound measurements in the volunteer study itself. It could be argued that this had relatively little impact on the implementation of the spinal curvature, since this shift in y direction only resulted in a minor shift in x direction, due to the curvature of the vertebrae's lamina, not in a substantial change in angle between two adjacent vertebrae. It is also reasonable to note that the ultrasound imaging visualizes the difference in reflecting properties —which means that the interface between bone and surrounding tissue is the most prominent in the image. The deviation in measurement location would thus not be hypothesized to affect the results to a larger extent.

5.2.1 Comparison to Additional Models

An additional model that was used for comparison was the UMTRI model, Figure A.1. As can be seen in this comparison, there was a resemblance in curvature, and the most prominent difference between the two was the more reclined posture of the UMTRI spinal curvature. When comparing the angles, the differences $\Delta\alpha$ were all $< 4°$, and largest in the location of the disc joining vertebra T8/T9, Table A.1. It is possible that the more reclined posture of the UMTRI model could be a consequence of a different pelvic and seat back angle as compared to the SAFER model.

The Izumiyama et al. average male curvature angles [15], Figure A.2, have been approximated according to the defined angles. This particular curvature showed close resemblance with the updated SAFER curvature in the thoracolumbar spine. One possible explanation to this could be due to the data being collected close in time to the Davidsson et al. data (publ. 2018 and 2026 respectively). The original SAFER curvature shared more similarities to the UMTRI data [20], collected during the 1980s. The data from UMTRI were also collected on U.S. population, while Izumiyama et al. collected data from Japanese occupants. This could also be a factor influencing the results. However, since the Davidsson et al. [31] data were collected in Sweden, it could be assumed that it was based on a population resembling the Swedish population, which raises the question if nationality, with the related behaviors, could be an influential factor. This is an opportunity for future research, to investigate if nationality affects factors such as spinal curvature, or if ethnicity might be a more influential parameter.

The skin back contour for the updated SAFER HBM was presented in Figure A.4, along the TU Delft model and the prediction model by Davidsson et al. The updated SAFER had more similarities with the prediction model than the original, Figure A.3 and A.4, but the characteristics in the cervical spine appeared to not have changed as clearly. One reason to why the change in skin back contour was not as clear as the change in lamina line could be due to the SAFER HBM having a smooth skin surface over the spinal column, which results in that the changes to the spinal column might not be reflected as prominently, since the skin is not as curved between the erector spinae muscles as they probably would be for an actual human. Since the changes in spinal curvature were relatively small (in the order of cm), it was considered unlikely that this would result in a deeper/narrower valley between the erector spinae muscles than what was present in the original SAFER HBM. This argument was supported by the results presented in Figure B.1, which showed that the skin to lamina distance of the SAFER HBM did not change substantially.

5.3 Updating the Curvature

As seen in Figure 4.3, the updated spinal curvature was of a slightly straighter nature in the thoracolumbar region, as compared to the original curvature. It was also visible that the updated curvature had less lordosis in the lower cervical spine and upper thoracic spine.

When closer examining the curvature, by presenting the absolute angle difference between the updated curvature and the prediction model, it became apparent that the implemented curvature was not exactly the targeted one. The angle difference at T12 was -0.6°, Table 4.3. Whilst this was an improvement as compared to the original angle difference of -8.3° (Figure 4.2), it was still not within the desired error range of ±0.5°. However, this error range was an arbitrary limit set by the authors of this thesis. The reason for this remaining difference was due to a contact arising between vertebrae T12 and L1 during the repositioning of the spine. It was not desired to deform any bones (i.e. treated as rigid), and thus this became a limitation to the update. When studying the remaining absolute angle differences, it can be seen that all other values were less than or equal to ±0.3° (compared to the target position of the spine that yielded a maximum deviation of -0.4°, Table 4.2) which was an accepted deviation. It could be argued that such angle differences might be realistic just from individual variations. One question that could be posed is to why the updated curvature was not exactly like the one in the prediction model, Figure 4.4. The hypothesis to why is that given limitations of the HBM, such as anatomical constraints that in a feasible way cannot be disregarded, some deviations from the exact prediction model should be accepted. Also, when applying a change in the orientation of a vertebra, the surrounding environment, such as muscle and fat tissue would be affected and deformed. This would introduce a change in orientation to the adjacent vertebra, meaning that the already changed orientation of an updated vertebra would be affected by changes to the adjacent vertebra. This introduced a small cascading effect that could not quite be regulated using this methodology, and seemed to be part of the explanation to the deviations from the prediction model.

An alternative to this method would be to instead translate the location of the vertebrae with respect to the desired lamina coordinates. This would require adjustment of the length between each segment of the prediction model and that of the SAFER HBM, which has no clear solution. The advantage of this alternative solution could be that it would provide for a methodology that would not demand for multiple iterations, given that no automatic morphing would occur if the articulation tool would not be used.

5.3.1 Coronal Plane Curvature

The original SAFER HBM is symmetric which means that the spine is straight in the coronal plane. The hypothesis was that if the curvature in the sagittal plane influenced how load was distributed, and how the structures responded to moments, a curvature in the coronal plane would also have an impact. The goal was to add a Cobb angle of 9° between vertebra T6 and T11. As presented in the result, the achieved Cobb angle was approximately 7°, which was a result of the anatomical constrains in the same way as when altering the curvature in the sagittal plane. The results from applying this curvature in simulation is presented in Section 5.4.

It was considered likely that some variation to the spinal curvature in the coronal plane is reasonable and would reflect a population that is not perfectly symmetric. This is an argument to why such characteristics should be reflected in HBMs, given that the goal is a biofidelic model of the human body. Creating asymmetrical models would be more complicated for the developers, which means that if such an effort were to be made, it needs to be certain that the value of the benefits would exceed the resources demanded —which cannot be motivated by this thesis, even though the results of this thesis presented that strain, force and moment is observed to differ between the different cases,supporting this suggestion.

Furthermore, adding a Cobb angle of 7°, would likely be a too drastic of a change if one were to implement variations in the coronal plane as default. In that case, a thorough study of a larger population would have to be done, e.g. with MRI scans to study the spinal posture. It would be desired for this population to not have a suspected scoliosis diagnosis but rather be classified as healthy in that matter. That sort of study would give a more representative view on spinal curvatures (in the coronal plane). With that being said, it might be difficult to fund such a project. The reason to highlighting this topic is that as mentioned earlier in this thesis, such data is sparse and recorded curvatures in the coronal plane (with scans or similarly) are usually retrieved from cohorts containing individuals with suspected scoliosis, which makes these data sets and statistics regarding it rather biased.

5.3.2 FE Model Quality

The maximum/minimum values of the mesh quality assessment metrics involving the spine were presented in Section 4.4. In Table 4.6, the solid element with the smallest Jacobian belongs to the so called "Thorax Spine to Internal Organs attachment", which is a form of connective tissue. One probable reason to why the Jacobian was decreased for the updated model and the model changed in coronal plane was due to the change of angles of the vertebrae creating some kind of inversion of the element, making it less than ideal. This could be the reason to why the resulting Jacobian was smaller than the original model's lowest value, that was found in the left pelvis innominate bone. As stated in Section 3.4.2, there are three criteria that can be used to assess the mesh quality regarding the Element Jacobian. The updated SAFER HBM and the coronal curvature SAFER HBM fulfill two out of three criteria, namely that the values are positive and greater than 0.2 in magnitude. However, the third criterion was not fulfilled, which was that less than 5% of the elements should have an Element Jacobian < 0.7. The values of the distributions were presented in Table D.6, where the percentages below 0.7 for the SAFER original is summed up to 6.60%, the updated to 6.66% and the coronal curvature to 6.74%.

Table 4.4 showed a large increase in the maximum warping of the updated models' shell elements. This regarded the part "Neck Soft Tissues Inner Null Left" (different elements for the two cases) which is a part surrounding the cervical vertebrae. This increase was likely due to the same reason as previously stated, namely the change of angles of the vertebrae which created a more warped element. Even though the maximum value was almost doubled, the quality was deemed reasonable, since warping is considered to be secondary to the AR and Element Jacobian, and the respective elements in question did not appear at the maximum AR or minimum Element Jacobian. The weakness in quality in a surrounding soft tissue should not affect the predicted vertebral body fracture risk, since it is based on the strain of the vertebral bone tissue. When reviewing the results for the solid elements presented in Table 4.7, the maximum warped element differed between models. The updated model's element was in the part called "Neck Soft Tissue", which is the element surrounding the previously mentioned shell part "Neck Soft Tissues Inner Null Left". All materials in Table 4.7 are soft tissues surrounding the spine, implying that the results of this thesis should not be affected since it is the vertebral body fracture risk that is evaluated.

In the original model, the most skewed element belonged to the part "Abdomen L5 Vertebra Cortical Posterior", Table 4.5, which is the bottom most vertebra. When updating the model with the curvature of the prediction model, the most skewed element belonged to "Thorax T12 Vertebra Cortical Posterior". The reason for this could be because of the changes that had to be made of the inferior articular processes of T12 to not get intersections between T12 and L1 in the simulation. If this would have been the case, the vertebrae would have been stuck together in an non-biofidelic manner. This reasoning was applied to the result for the updated model in Table 4.8 as well, since that was for the corresponding trabecular bone. With the changes in the coronal plane, the most skewed element was in the "Thorax T2 Vertebra Cortical Posterior" instead. The reasoning to why follows the already presented hypothesis. After repositioning the HBM, some intersections were created. This resulted in some postprocessing that included some direct form morphing, which is the likely explanation to the decrease in element quality in this case. The maximum skewness for the solid elements of the model was found in the "Thorax Rib Intercostal Muscle Inner", which was also morphed to avoid intersections in the model. To conclude the model quality assessment, it was concluded that the soft tissues having the largest extreme values should not have affected the results of the application study. The weaker elements found in the inferior articular processes of the vertebrae should not have had a substantial impact on the straining since they are not part of the load bearing parts of the spine (i.e. the vertebral bodies and intervertebral discs).

5.4 Application Study

The updated, and coronal, spinal curvature of the SAFER HBM were evaluated by paired simulations with baseline and updated, or coronal, spinal curvatures. In this section, the comparison of the baseline to updated model will be discussed first, followed by a discussion of the differences and similarities to the then implemented coronal plane curvature. Initially, variations of frontal impacts were simulated and while analyzing these, it came to light that the differences between baseline and updated simulation results were similar, as presented with the peak strain in Figures 4.8, 4.11. When studying the run-off road scenarios, it became apparent that an impact with a larger compressive force exerted on the vertebrae produced interesting results. For both run-off road (1) and run-off road (2), there was a clear increase in force exerted on the vertebrae after the spinal curvature update, for both the driver and passenger, Figures 4.13, 4.16, which was most prominent for the position that was mostly affected by the roll motion.

When the compressive force (Fz-), in the moment of impact is exerted on the spine, the force travels in the spine from a caudal to cranial matter. The force from the impact is distributed in the body. The compressive force mostly of interest in this thesis would likely to some extent propagate along the spine, to some extent to the next disc (where some of it would be absorbed) and onto the next vertebrae, while some of the force would be distributed into surrounding tissue. The updated spinal curvature was more straight than the original SAFER HBM. In the case of a more curved spine, the hypothesis is that the force component propagating along the spine would be of smaller magnitude, given that some of the vertical force, that is the force component distributing force into the surrounding tissue, would propagate outside the spinal column. The opposite would stand for the more straight spine, as described in Figure 5.1. This reasoning would also explain why the peak force is largest in vertebra L5, since the force has yet to be distributed anywhere else, together with the fact that vertebra L5 carries more weight from the spine and body as compared to more superior vertebrae.

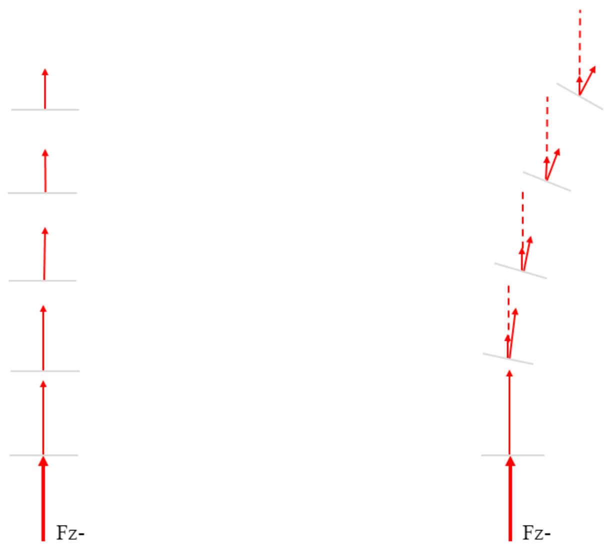

Figure 5.1: Hypothesized load distribution.

If this hypothesis were to be true, it would mean that more force is kept in the direction along the spine in the updated model, thus resulting in the increase seen in the peak force figures presented. This could imply that the magnitude of force has been underestimated with the previous curvature of the spine. There have been previous studies [47, 48], demonstrating that compressive force could be used as an injury predictor for vertebral fractures, which means that it is important to capture this accurately. That result is also confirmed by the linear regression model created in this thesis, implying that force has a linear relationship with strain, Figure 4.25, 4.26. It has previously been hypothesized that a straighter spine could take more load [3], which would imply that this increase in compressive force would not on its own contribute to an increased strain and therefore an increased risk of injury. This statement does not hold for all observations made in this thesis, at least not in the locations of vertebra T6 and L1. The results from the linear regression models, Figures 4.25,4.26, imply that there is a significant linear relationship between the strain and compressive force.

However, the linear regression model created for vertebra L5 does not support this hypothesis. For the updated curvature, the relationship between force and strain is significant, given $p < 0.05$, unlike the baseline case. But, the relationship did not seem to be modelled quite accurately given the low R^2 value.

Consistent for all load cases was that a clear pattern could be observed between flexion moment (My+) and strain. When studying the peak strain and peak My+ figures, as for the run-off road (1) impact (Figure 4.14), it was apparent that when the y moment increased, so did the strain. I.e., whenever there was a peak in the y moment, there was a peak in strain. This finding was confirmed by the linear regression models for vertebra T6, L1 and L5 and the relationship is probable to hold for all vertebrae in the thoracic and lumbar spine. For all linear regression models, the relationship between My+ and strain was determined to be significant, and modelled well by a linear relationship especially for vertebra T6 and L1. For that of L5, the model did not capture the variation as well. To reason about why, it seems as if the data for vertebra T6, L1 present relationships that are highly linear and to why the results from the same analysis with data from vertebra L5 was more diffuse, the answer could be the variation in the data of vertebra L5. This variation could be a consequence of noise, or due to the different impacts creating moments and force that initially were of large magnitude and with large differences in characteristics, whilst more cranially in the spine, the effect of these initial characteristics of the loading and moments had leveled out.

After varying the spinal curvature in the coronal plane as well, the same observations regarding the frontal and oblique impacts were made. Regarding the run-off road impacts, more interesting results were found. The force was increased with the coronal variations as compared to the baseline case, as was seen for the updated model. This held true for all vertebrae except T7 (in run-off (1)). Noted was that the force seemed to increase less as compared to the baseline with the coronal variations than in the previous case, when changes were only made in the sagittal plane.

When reasoning about the difference between only updating the curvature in the sagittal plane (referred to as updated model) and additionally varying the coronal plane, the difference was most apparent in the region between vertebra T6 and T11. This was reasonable, since it was the region where the coronal curvature variation was implemented. Between these vertebrae, the peak force was much closer to the baseline case as compared to when the updates were only made in the sagittal plane. When introducing a curvature in the coronal plane, the spine was forced to take on a more curved posture (but in another plane), and reasoning as previously this might introduce further distribution of forces into the surrounding tissue, resulting in less force propagating along the spine. This also held true for run-off road (2). This was supported by the internal energies in Table G.1, Appendix G, especially for FSU T5/T6, but also for FSU T12/L1. When comparing the updated curvature and the coronal plane curvature, there was a 24% increase of internal energy in T5/T6 for the updated, straighter curvature, Appendix G. The difference between the updated curvature and the original SAFER HBM curvature was even bigger, resulting in a 40% increase in the straighter case. The same pattern was consistent for T12/L1 as well, although smaller in magnitude (8% and 18% respectively). As previously stated, vertebra L5, and thus FSU L4/L5, deviated from the rest of the spine, not following the presented pattern. Regarding the internal energy, the hypothesis is that the force is distributed between compressive force (Fz-) and moments, most likely My+. One possible explanation to why the pattern was consistent in the thoracic spine could be that the force/energy dissipates into the ribs, which is not a possibility for the lumbar vertebrae. Considering the size of the most caudal, lumbar vertebrae, they should be able to endure higher stresses than smaller vertebrae, which is a likely explanation to the higher values in Table G.1.

Studying the peak strain for run-off road (1), the coronal variation introduced a difference primarily in vertebra T11, which was increased in strain as compared to the baseline and updated versions (both for driver and passenger), Figures 4.22, F.1. This peak in strain could not solely be explained by the y moment, which was the pattern previously seen. For run-off road (2), the y moment was increased in the coronal curvature as compared to the updated alone between vertebra T9 and T11, but the strain was reduced. This could have been due to the reduced compressive force in the coronal plane curvature, in comparison to when only changing the sagittal plane curvature, Figures 4.16, 4.23.

Linear regression models were created for the coronal curvature as well to investigate whether the same relations held for a spine that was curved in both the sagittal and coronal plane. The results of these were roughly the same as for the updated model, the relations thus seemed to hold as for the updates in the sagittal plane. This result could imply that these linear relationships are stable, given that they do not change when introducing new data with more variations. For this case, it was again observed that the results of vertebra L5 differed from those of vertebra T6 and L1, and does not support the statement that the force and strain has a linear relationship (in baseline nor coronal curvature), Figures E.1, E.2, E.3.

5.5 Injury risk

In this thesis, the risk referred to is, as previously presented, a fracture risk that arise in a vertebral body due to compressive strain along the vertical vertebrae body axis. It has also been presented that this strain could arise from both bending moments and compressive force. As seen in force and moment figures, the compressive force and/or bending moment were not constant over the spine. For instance in the run-off road cases, the peak compressive force was lower in the upper regions and higher in the lower regions of the spine. As presented previously, regarding the internal energy of the vertebrae, this reduced force in more cranial vertebrae was hypothesized to not only be due to the more cranial vertebrae carrying less weight of the body, but also due to some of the strain energy being directed through other structures.

The injury risk function for vertebral body fracture [6] gives one risk prediction per vertebra. However, an open question that remains is if vertebral fracture risk should be investigated as a coupled injury risk or not. Given that the vertebrae are coupled together and form a system, the question is what happens if stability is lost in the system by fracture of one or more vertebrae. Comparing this to rib fractures, where multiple fractures would indicate a loss of stability in the ribcage, which could increase the risk of other fractures. A similar reasoning might be possible to apply to the spine, but then the question regarding if the spine should be modelled as a system of series or parallel connected spring arises. Since the vertebrae are connected in a chain like manner, it could be argued to view the system as coupled in series, to the largest extent at least. It should be noted, that since the spine is in its turn coupled to the rest of the skeleton and therefore the rest of the body, the issue is not quite so simple.

For each individual vertebra, treated as an isolated system, one could argue that one fracture would increase the risk for a subsequent one given the damage to the structure. But, if for example vertebra L5 were to be fractured, as seen most likely in this thesis, this might also affect the risk of fracture in more cranial vertebrae. When one vertebra is fractured, it could be assumed that energy is released. That would indicate that less energy would be transferred into the next vertebra, which would indicate a lower risk for fracture in that location. However, reasoning as with the ribcage, a fracture could possibly reduce the stability of the system and instead increase the risk of injury, even though the amount of force exerted on that vertebra may be slightly reduced. It could also be argued that when a fracture arises in a vertebra, that component in our system may have less capacity to carry load and the stress might be increased on the remaining components in the system. With this presented reasoning, the conclusion is that the fracture risk should eventually also be investigated on a system level as well as locally for each vertebra. This is deemed outside the scope of this thesis, but future research within this area could be done.

5.6 Conclusion

The spinal curvature of the prediction model representing a volunteer cohort, was straighter than that of the SAFER HBM v12. The goal thus became to remodel the SAFER spinal curvature with less lordosis in the upper thoracic spine and less kyphosis in the thoracolumbar spine.

The angles between the vertebrae segments were compared between the HBM and the prediction model from volunteer data and updates were made based on the differences. It was concluded during the work that given the restraints that were placed on the HBM, it was not possible to entirely reposition the SAFER spine into the target position, but the result was accepted as reasonably close. Furthermore, an investigation into spinal curvature in the coronal plane was made, and it was seen that the results from the application study differed between the coronal curvature and that of the curvature only altered in the sagittal plane. It seemed as if the more curved position of the coronal curvature led to slightly reduced compressive force of the vertebrae.

Another conclusion that could be made was that the vertebral body trabecular bone inferior-superior strain seemed to be correlated to the flexion of the spine, and to some extent the inferior-superior compressive force as well. It seemed as if this flexion was the strongest predictor for the increased vertebral strain. Compressive force seemed to also be a reasonable predictor for the increased strain. Furthermore, it was concluded that a more curved spine was subject to less compressive force by interpreting the results, possibly due to that the load distribution pattern differed from the spine with straighter posture.

The strain of the coronal plane curvature was not as easily determined as dependent of the flexion. By the results of the linear regression, it could be seen that the strain and flexion still had a linear relationship for this case, but the peak strain values were more irregular than those of the sagittal curvature, which implied that other factors may have a substantial impact on the results. This could, in some cases, be due to the peak compressive force having a larger impact on the strain.

Bibliography

[1] World Health Organization, "Road traffic injuries," 2023. Accessed: May 12, 2026.

[2] A. Kullgren, H. Stigson, and M. Krafft, "Development of whiplash associated disorders for male and female car occupants in cars launched since the 80s in different impact directions," in *Proceedings of the International Research Council on the Biomechanics of Injury (IRCOBI) Conference*, no. IRC-13-14, pp. 51–62, IRCOBI, 2013.

[3] L. Jakobsson, T. Bergman, and L. Johansson, "Identifying thoracic and lumbar spinal injuries in car accidents," in *Proceedings of the International Research Council on the Biomechanics of Injury (IRCOBI) Conference*, 2006.

[4] R. D. Rao, C. A. Berry, N. Yoganandan, and A. Agarwal, "Occupant and crash characteristics in thoracic and lumbar spine injuries resulting from motor vehicle collisions," *The Spine Journal*, vol. 14, pp. 2355 – 2365, 2014.

[5] L. Jakobsson, M. Björklund, and A. Westerlund, "Thoracolumbar spine injuries in car crashes," in *Proceedings of the International Research Council on the Biomechanics of Injury (IRCOBI) Conference*, no. IRC-16-22, IRCOBI, 2016.

[6] J. Iraeus, Y. N. Poojary, L. Jaber, J. John, and J. Davidsson, "A new open-source finite element lumbar spine model, its tuning and validation, and development of a tissue-based injury risk function for compression fractures," in *Proceedings of the International Research Council on the Biomechanics of Injury (IRCOBI) Conference*, no. IRC-23-132, pp. 1180–1191, IRCOBI, 2023.

[7] R. Cutlan, M. Khokhar, N. Shammout, A. S. Shah, L. Frazer, N. Yoganandan, B. S. Shender, J. Sheehy, G. Paskoff, D. Nicolella, T. Bentley, S. Shabani, and B. D. Stemper, "Lumbar spine orientation affects compressive fracture outcome," *Annals of Biomedical Engineering*, vol. 54, no. 4, pp. 1076–1085, 2026.

[8] L. Tang, J. Zheng, and J. Hu, "A numerical investigation of factors affecting lumbar spine injuries in frontal crashes," *Accident Analysis and Prevention*, vol. 136, 2020.

[9] B. Pipkorn, J. Östh, J. Iraeus, and K.-J. Larsson, *SAFER HBM AM50 V12 Occupant Manual*. SAFER Vehicle and Traffic Safety Centre, version 12 ed., 2026.

[10] E. Brynskog, "SAFER HBM model development for enhanced submarining prediction," tech. rep., Department of Mechanics and Maritime Sciences, Chalmers University of Technology, 2024.

[11] K.-U. Schmitt, P. F. Niederer, D. S. Cronin, B. Morisson, M. H. Muser, and F. Walz, *Trauma Biomechanics*. Springer, 2019. Fifth Edition.

[12] J. A. Waxenbaum, V. Reddy, and B. Futterman, "Anatomy, back, intervertebral discs," in *StatPearls*, Treasure Island, FL: StatPearls Publishing, 2026.

[13] H. Gray, *Anatomy of the Human Body*. 1918. Bartleby's Online Edition.

[14] B. Pipkorn, L. Jakobsson, J. Iraeus, and J. Östh, "The SAFER HBM – a human body model for seamless integrated occupant analysis for all road users," in *Proceedings of the 27th International Technical Conference on the Enhanced Safety of Vehicles (ESV)*, no. 23-0242, National Highway Traffic Safety Administration, 2023.

[15] T. Izumiyama, N. Nishida, H. Iwanaga, X. Chen, J. Ohgi, K. Mori, T. Hayashi, I. Sakuramoto, R. Asahi, S. Sugimoto, and M. Ueno, "The analysis of an individual difference in human skeletal alignment in seated posture and occupant behaviour using HBMs," in *Proceedings of the International Research Council on the Biomechanics of Injury (IRCOBI) Conference*, no. IRC-18-84, pp. 549–560, 2018.

[16] H. Li and Y. Wang, "Influence of spinal curvature variations on driver kinematics and injury risk in frontal impact." PowerPoint presentation, 2015. Tianjin University of Science and Technology.

[17] F. Sato, M. Odani, Y. Miyazaki, T. Nakajima, J. Antona Makaoshi, K. Yamazaki, K. Ono, M. Svensson, J. Östh, S. Morikawa, S. Schick, and A. Ferrerio Perez, "Investigation of whole spine alignment patterns in automotive seated posture using upright open MRI systems," in *Proceedings of the International Research Council on the Biomechanics of Injury (IRCOBI) Conference*, no. IRC-16-23, 2016.

[18] A. Tomezzoli, A. Agouram, B. Chalamet, J.-B. Pialat, S. Duprey, V. Cunin, and B. Fréchède, "Predicting cervico-thoraco-lumbar vertebra positions from cutaneous markers: Combining local frame and postural predictors improves robustness to posture," *Journal of Biomechanics*, vol. 164, p. Article 111961, 2024.

[19] L. W. Schneider, D. H. Robbins, M. A. Pflug, and R. G. Snyder, "Development of anthropometrically based design specifications for an advanced adult anthropomorphic dummy family, volume 1," Tech. Rep. UMTRI-83-52-1, University of Michigan Transportation Research Institute, Ann Arbor, MI, USA, 1983.

[20] D. H. Robbins, "Anthropometric specifications for mid-sized male dummy, volume 2," Tech. Rep. UMTRI-83-53-2, University of Michigan Transportation Research Institute, Ann Arbor, MI, USA, 1983.

[21] A. Bokdam, G. Vledder, Y. W. Song, and P. Vink, "Human back contour modeling for backrest design in future vehicles," *Applied Ergonomics*, vol. 133, p. Article 104700, 2026.

[22] A. A. White and M. M. Panjabi, *Clinical Biomechanics of the Spine*. Philadelphia: J. B. Lippincott Company, 2 ed., 1990.

[23] R. Cutlan, M. Khokhar, N. Shammout, A. S. Shah, L. Frazer, N. Yoganandan, B. S. Shender, J. Sheehy, G. Paskoff, D. Nicolella, T. Bentley, and S. Shabani, "Lumbar spine orientation affects compressive fracture outcome," *Annals of Biomedical Engineering*, vol. 54, no. 4, pp. 1076–1085, 2026.

[24] L. Jakobsson, M. Björklund, and A. Westerlund, "Thoracolumbar spine injuries in car crashes," in *Proceedings of the International Research Council on the Biomechanics of Injury (IRCOBI) Conference*, no. IRC-16-22, 2016.

[25] F. A. Pintar, N. Yoganandan, D. Maiman, M. Scarboro, and R. W. Rudd, "Thoracolumbar spine fractures in frontal impact crashes," *Annals of Advances in Automotive Medicine*, vol. 56, pp. 233–248, 2012.

[26] L. Jakobsson, M. Björklund, and A. Axelson, "Vertical occupant loading in car crashes: Test methods and countermeasures," in *SAE Technical Paper*, SAE International, 2015.

[27] S. M. Duma, A. R. Kemper, D. M. McNeely, P. G. Brolinson, and F. Matsuoka, "Biomechanical response of the lumbar spine in dynamic compression," *Biomedical Sciences Instrumentation*, vol. 42, pp. 443–448, 2006.

[28] M.-H. Horng, C.-P. Kuok, M.-J. Fu, C.-J. Lin, and Y.-N. Sun, "Cobb angle measurement of spine from X-ray images using convolutional neural network," *Computational and Mathematical Methods in Medicine*, 2019.

[29] D. Hayashi, N.-E. Regnard, J. Ventre, V. Marty, L. Clovis, L. Lim, N. Nitche, Z. Zhang, A. Tournier, A. Ducarouge, A. J. Kompel, C. Tannoury, and A. Guermazi, "Deep learning algorithm enables automated Cobb angle measurements with high accuracy," *Skeletal Radiology*, vol. 54, no. 7, pp. 1383–1392, 2025.

[30] S. Wang, M. Li, J. Ren, J. Tao, M. Fang, and L. Kong, "Global prevalence and associated risk factors of scoliosis in children and adolescents: A systematic review and meta-analysis," *BMC Public Health*, vol. 25, 2025.

[31] J. Davidsson, Y. Wang, J. Östh, and J. Iraeus, "Statistical model of the spine, head, and extremities in a modern car seat. manuscript in preparation," 2026. Chalmers University of Technology.

[32] T. A. Burkhart, D. M. Andrews, and C. E. Dunning, "Finite element modeling mesh quality, energy balance and validation methods: A review with recommendations associated with the modeling of bone tissue," *Journal of Biomechanics*, vol. 46, no. 9, pp. 1477–1488, 2013.

[33] C. E. Quenneville and C. E. Dunning, "Development of a finite element model of the tibia for short-duration high-force axial impact loading," *Computer Methods in Biomechanics and Biomedical Engineering*, vol. 14, no. 2, pp. 205–212, 2011.

[34] C. A. Felippa, “FEM modeling: Mesh, loads and BCs,” in *Introduction to Finite Element Methods*, ch. 7, Boulder, CO: University of Colorado Boulder, 2012.

[35] P. M. Knupp, “Remarks on mesh quality,” in *Proceedings of the 45th AIAA Aerospace Sciences Meeting and Exhibit*, no. AIAA-2007-257, (Reno, NV, USA), 2007.

[36] C. Untaroiu, K. Darvish, J. Crandall, B. Deng, and J.-T. Wang, “A finite element model of the lower limb for simulating pedestrian impact.,” *Stapp Car Crash Journal*, vol. 49, pp. 157–181, 2005.

[37] Z. Li, J. Hu, M. P. Reed, J. D. Rupp, C. N. Hoff, J. Zhang, and B. Cheng, “Development, validation, and application of a parametric pediatric head finite element model for impact simulations,” *Annals of Biomedical Engineering*, vol. 39, no. 12, pp. 2984–2997, 2011.

[38] M. H. Ray, M. Mongiardini, A. O. Atahan, C. A. Plaxico, and M. Anghileri, “Recommended procedures for verification and validation of computer simulations used for roadside safety applications,” pp. 22–24, 2008. Technical guideline.

[39] BETA CAE Systems, *ANSA User Guide: Chapter 10 – Surface Meshing and Shell Mesh*. BETA CAE Systems, version 24 ed., 2024. Software user manual.

[40] M. P. Reed, M. A. Manary, C. A. C. Flannagan, and L. W. Schneider, “A statistical method for predicting automobile driving posture,” *Human Factors: The Journal of the Human Factors and Ergonomics Society*, vol. 44, no. 4, pp. 557–568, 2002.

[41] M. P. Reed, S. M. Ebert, M. L. Jones, and J. J. Hallman, “Prevalence of non-nominal seat positions and postures among front-seat passengers,” *Traffic Injury Prevention*, vol. 21, no. sup1, pp. S7–S12, 2020.

[42] L. Jakobsson, M. Lindman, A. Axelson, B. Lokensgard, M. Petersson, B. Svanberg, and J. Kovaceva, “Addressing run off road safety,” *SAE International Journal of Passenger Cars – Mechanical Systems*, vol. 7, no. 1, pp. 505–514, 2014.

[43] NumPy Developers, “numpy.polyfit.” `https://numpy.org/doc/stable/reference/generated/numpy.polyfit.html`. Accessed: May 7, 2026.

[44] NumPy Developers, “numpy.polyval.” `https://numpy.org/doc/stable/reference/generated/numpy.polyval.html`. Accessed: May 7, 2026.

[45] The SciPy Community, “scipy.stats.linregress.” `https://docs.scipy.org/doc/scipy/reference/generated/scipy.stats.linregress.html`. Accessed: May 7, 2026.

[46] J. Urrutia, P. Besa, F. Narvaez, A. Meissner-Haecker, C. Rios, and C. Piza, “Mid and lower thoracic kyphosis changes during adulthood: The influence of age, sex and thoracic coronal curvature,” *Archives of Orthopaedic and Trauma Surgery*, vol. 142, no. 8, pp. 1731–1737, 2022.

[47] S. K. Tushak, B. D. Gepner, J. L. Forman, J. J. Hallman, B. Pipkorn, and J. R. Kerrigan, “Human lumbar spine injury risk in dynamic combined compression

and flexion loading," *Annals of Biomedical Engineering*, vol. 51, no. 6, pp. 1300–1314, 2023.

[48] M. Ortiz-Paparoni, J. Op 't Eynde, J. Kait, B. Bigler, J. Shridharani, A. Schmidt, C. Cox, C. Morino, F. Pintar, N. Yoganandan, J. Moore, J. Zhang, and C. R. Bass, "The human lumbar spine during high-rate under seat loading: A combined metric injury criteria," *Annals of Biomedical Engineering*, vol. 49, no. 11, pp. 3018–3030, 2021.

A

Additional Models for Comparison

A.1 UMTRI

Additionally, the UMTRI prediction model was included for comparison in this thesis to expand the scope [20], namely the vertebral disc center line. The comparison of the SAFER original curvature and the UMTRI spinal curvature (Table 19 [20], Figure 5-1 [19]) was presented in Figure A.1. As could be seen, these curvatures closely resembled each other, Table A.1. Measurement locations for the SAFER HBM were joint locations of C7/T1, T4/T5, T8/T9, T12/L1, L2/L3, L5/S1 (posterior on discs), which corresponded roughly to the locations presented in the UMTRI study.

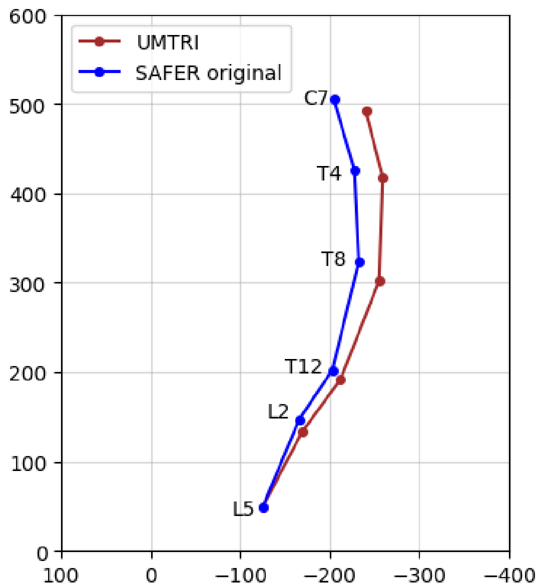

Figure A.1: The spinal curvature from the UMTRI study [20] as compared to the original SAFER curvature.

Table A.1: Angles between UMTRI and SAFER original (°), rounded to one decimal.

Joint location (disc)	SAFER	UMTRI	$\Delta\alpha$
T4/T5	12.3	14.4	-2.1
T8/T9	-5.5	-2.0	-3.5
T12/L1	-18.0	-21.4	3.4
L2/L3	-34.9	-36.1	1.2
L5/S1	-25.0	-27.7	-2.7

A.2 Izumiyama et al.

Figure A.2 shows an example of a curvature derived from the angles specified in Izumiyama et al. [15] with comparison to the original SAFER as well as the updated SAFER curvature. The displayed vertebrae are C3—S1. The curvature was derived using the angles specified for the average of the male population in Appendix Table 1 [15]. The angles were implemented into the SAFER HBM using the previously mentioned Articulation tool (spine) in ANSA. The angles were altered iteratively to find a position mimicking the curvature of the average male angles presented by Izumiyama et al. The magnitude of the angles between vertebrae of interest, Figure 2.6, were measured in the HBM by using the ANSA Measure tool (angle between vectors). Since there were many degrees of freedom, and each angle was only specified using two vertebrae, there could have been many different curvatures that corresponds to these angles. Thus, this was not the only curvature fulfilling the requirements. However, it was one of them. Visually, it could be stated that the average male curvature from Izumiyama et al. was closer to the curvature of the updated SAFER HBM than the original. The PA differed with 0.49°.

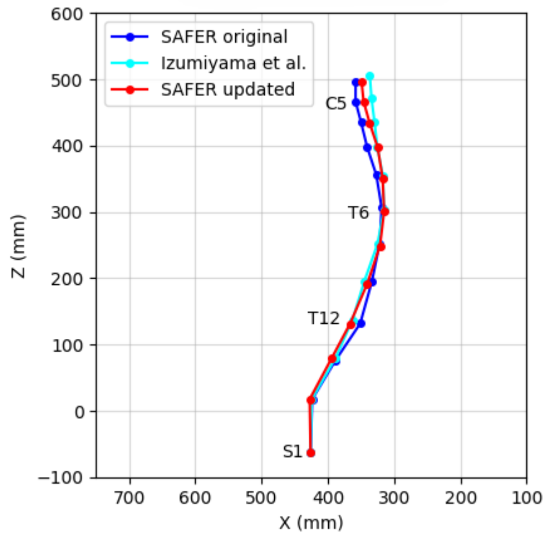

Figure A.2: An average male spinal curvature derived from angles published by Izumiyama et al. [15] as compared to the original SAFER curvature and updated SAFER curvature.

A.3 Bokdam et al.

The skin back contour of the SAFER HBM and the prediction model by Davidsson et al. [31] comparison, showed that when curvatures are aligned at the lowest measuring point (LMP) which should correspond to the S1 marker, the original SAFER HBM had a more curved neck than the prediction model, Figure A.3. While, in comparison with the Bokdam et al. study, the back angle was completely different, making a direct comparison difficult. The Bokdam et al. prediction model was rotated 15° clockwise around the inferior point to compensate for differences in the seated positioning setups.

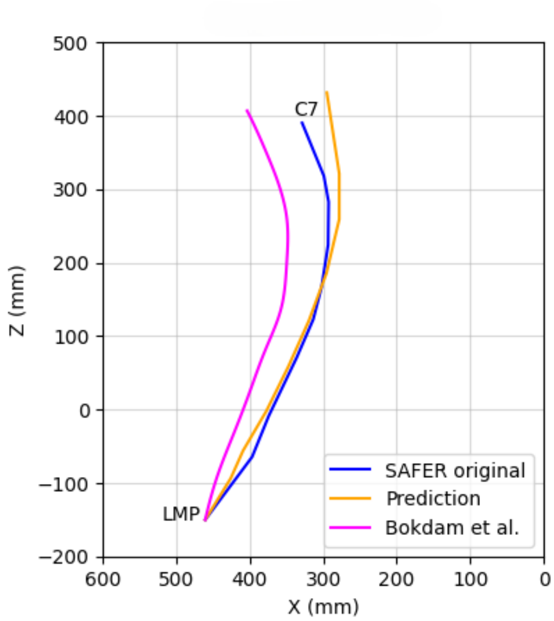

Figure A.3: The back contours of the original SAFER HBM, the prediction model and Bokdam et al. [21].

The updated skin back contour is presented in Figure A.4, along with the prediction model and the TU Delft model by Bokdam et al.

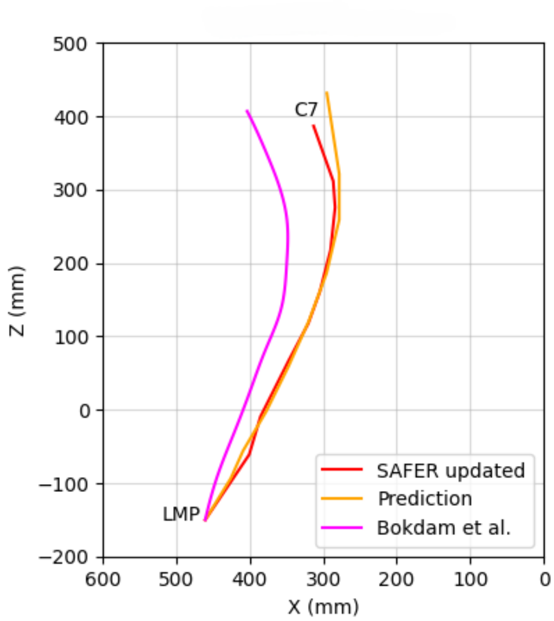

Figure A.4: The back contours of the updated SAFER HBM, the prediction model and Bokdam et al.

B

Skin to Lamina Distance

Table B.1: Distance between skin and lamina in x-direction (mm).

Vertebra location	SAFER original	Prediction	SAFER updated
C3	47	36	54
C5	52	37	57
C7	47	40	50
T2	67	46	65
T4	60	38	60
T6	51	19	52
T8	45	1	43
T10	46	10	47
T12	45	15	46
L2	40	17	36
L4	53	2	53
S1	9	24	8

The skin to lamina x distance of the updated SAFER HBM was similar to the original SAFER, and was larger than the prediction model in all cases except for S1/Pin 1. The distances in x direction between lamina and skin for SAFER HBM and the predicted model, Figure B.1.

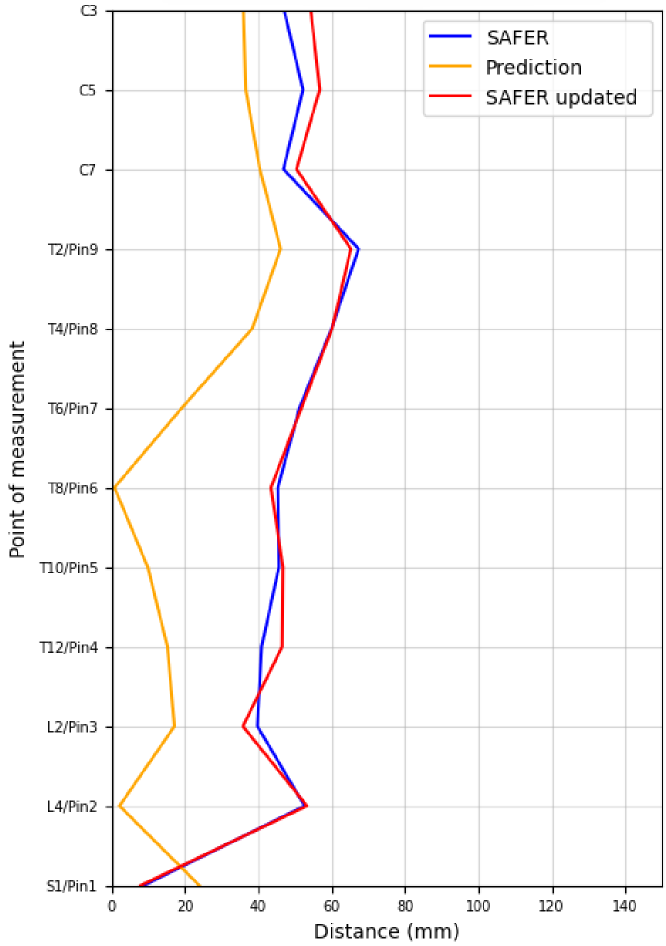

Figure B.1: Distance between the lamina and skin in x direction for the original and updated SAFER, as well as the prediction model.

C

Update Including Pelvic Angle

During the thesis it became apparent that when constraining both the pelvis and head location, the spine could not quite take the desired position and contacts between vertebra T12 and L1 arose. This issue was solved by introducing an small angle to the facet joints of vertebra T12. To investigate whether this contact did in fact result from the constraining of the model, an attempt was made to alter the PA. This resulted in an angle difference that was more comparable to the final result presented in Section 4, where the facet joints were altered, than the SAFER HBM with restrained pelvis and unchanged facets, C.2. This result is included to show that by constraining the pelvis, which was desired, the spine cannot simply move into any desired position. The angle differences for this result are presented in Table C.1.

Table C.1: Actual differences in angles between vertical line and vertebrae when including alterations to the PA, rounded to one decimal.

Vertebrae	SAFER updated w. PA	Predicted	Angle Difference
C5	6.0	6.0	0.0
C7	15.6	15.6	0.0
T2	18.1	18.2	0.1
T4	9.3	9.4	0.1
T6	3.0	2.2	-0.8
T8	-7.3	-6.7	0.6
T10	-18.1	-18.3	-0.2
T12	-22.8	-23.9	-1.1
L2	-29.6	-28.0	1.6
L4	-28.3	-28.0	0.3
S1	-11.7	-11.9	-0.2

Table C.2: Actual differences in angles between vertical line and vertebrae with unchanged facets and unchanged PA, rounded to one decimal.

Vertebrae	SAFER Updated wo. PA	Predicted	Angle Difference
C5	6.0	6.0	0.0
C7	15.7	15.6	-0.1
T2	18.2	18.2	0.0
T4	9.3	9.4	0.1
T6	2.5	2.2	-0.3
T8	-6.9	-6.7	0.2
T10	-18.5	-18.3	0.2
T12	-21.5	-23.9	-2.4
L2	-30.1	-28.0	2.1
L4	-28.2	-28.0	0.2
S1	0.9	-11.9	-12.8

D

Model Quality

D.1 Shell Elements

Table D.1: Aspect ratio distribution for the original, updated and coronal plane curvature FE model.

AR interval	Original FE model (%)	Updated FE model (%)	Coronal plane curvature model (%)
0-2	87.53	87.82	87.76
2-3	10.55	10.33	10.35
3-4	1.53	1.48	1.49
4-5	0.28	0.26	0.29
5-10	0.12	0.11	0.11

Table D.2: Element Jacobian distribution for the original, updated and coronal plane curvature FE model.

Jacobian interval	Original FE model (%)	Updated FE model (%)	Coronal plane curvature FE model (%)
<0.5	0.08	0.08	0.08
0.5-0.6	0.44	0.45	0.45
0.6-0.7	1.57	1.57	1.62
0.7-0.8	5.22	5.26	5.36
0.8-0.9	13.30	13.51	13.71
0.9-1.01	79.38	79.13	78.77

Table D.3: Warping distribution for the original, updated and coronal plane curvature FE model.

Warping interval	Original FE model (%)	Updated FE model (%)	Coronal plane curvature FE model (%)
0-2	73.96	73.46	72.94
2-4	14.45	14.38	14.52
4-6	5.62	5.87	5.88
6-8	2.80	2.93	3.01
8-10	1.56	1.64	1.67
10<	1.61	1.72	1.99

Table D.4: Skewness distribution for the original, updated and coronal plane curvature FE model.

Skewness interval	Original FE model (%)	Updated FE model (%)	Coronal plane curvature FE model (%)
0-18	78.01	77.70	77.54
18-36	18.78	19.22	19.13
36-45	2.51	2.36	2.56
45-72	0.70	0.72	0.76

D.2 Solid Elements

Table D.5: Aspect ratio distribution for the original, updated and coronal plane curvature FE model.

AR interval	Original FE model (%)	Updated FE model (%)	Coronal plane curvature FE model (%)
0-2	61.63	61.76	61.68
2-4	33.85	33.73	33.76
4-6	3.79	3.77	3.84
6-8	0.66	0.67	0.66
8-10	0.07	0.07	0.07

Table D.6: Element Jacobian distribution for the original, updated and coronal plane curvature FE model.

Jacobian interval	Original FE model (%)	Updated FE model (%)	Coronal plane curvature FE model (%)
<0.5	0.12	0.13	0.13
0.5-0.6	0.98	0.99	1.01
0.6-0.7	5.55	5.57	5.60
0.7-0.8	11.95	11.99	12.06
0.8-0.9	31.73	31.94	32.03
0.9-1.01	49.66	49.38	49.17

Table D.7: Warping distribution for the original, updated and coronal plane curvature FE model.

Warping interval	Original FE model (%)	Updated FE model (%)	Coronal plane curvature FE model (%)
0-2	47.11	46.27	45.87
2-4	23.44	23.55	23.53
4-6	11.47	11.78	11.80
6-8	6.96	7.14	7.20
8-10	4.90	4.97	5.05
10<	6.12	6.29	6.55

Table D.8: Skewness distribution for the original, updated and coronal plane curvature FE model.

Skewness interval	Original FE model (%)	Updated FE model (%)	Coronal plane curvature FE model (%)
0-2	0.21	0.22	0.21
2-4	1.40	1.39	1.36
4-6	3.25	3.17	3.05
6-8	4.62	4.54	4.45
8-10	5.56	5.55	5.50
10<	84.95	85.12	85.43

E

Linear Regression Model: Coronal Plane Curvature

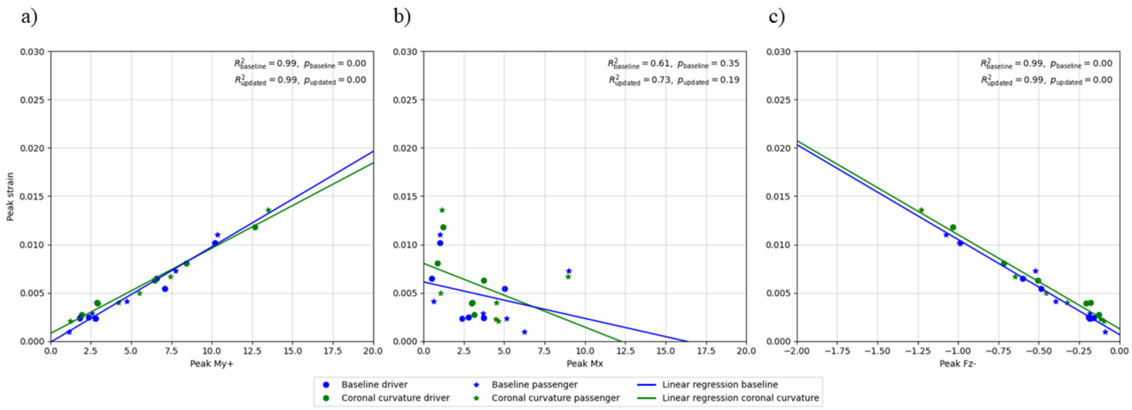

Figure E.1: The linear regression between strain and chosen variables for vertebra T6, for the coronal curvature.

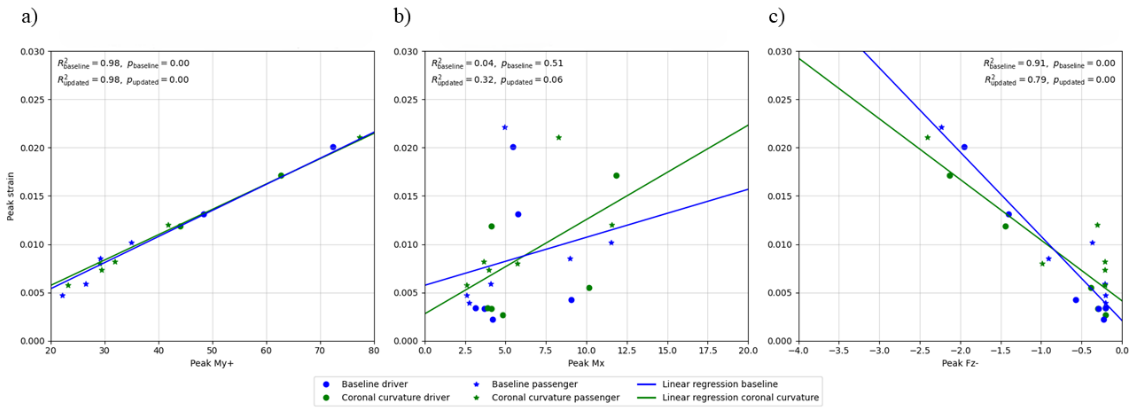

Figure E.2: The linear regression between strain and a) y moment, b) x moment, c) compressive force for vertebra L1, for the coronal curvature.

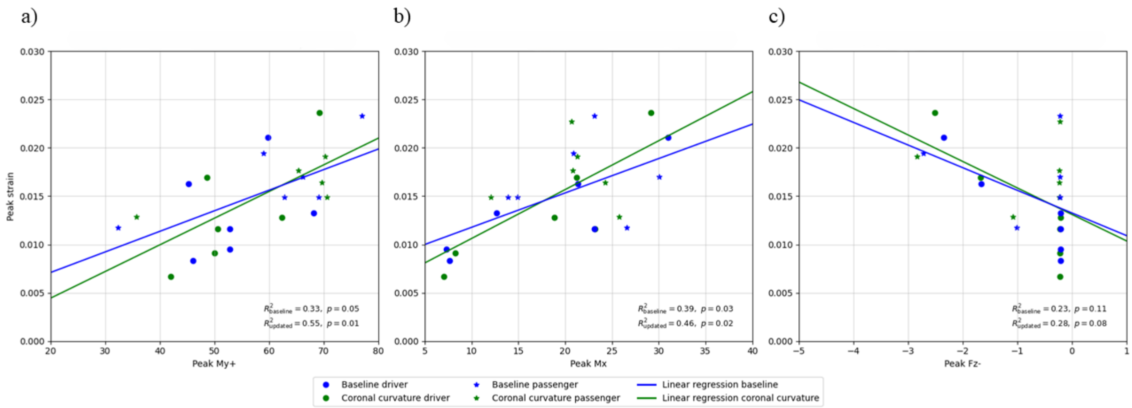

Figure E.3: The linear regression between strain and and a) y moment, b) x moment, c) compressive force for vertebra L5, for the coronal curvature.

F

Comparison Between Updated and Coronal Plane Curvature

To more clearly visualize the differences in vertebral strain recorded in simulation with a spine updated in only the sagittal plane as compared to updated in the sagittal and coronal plane, this visualization was included to exemplify, Figure F.1.

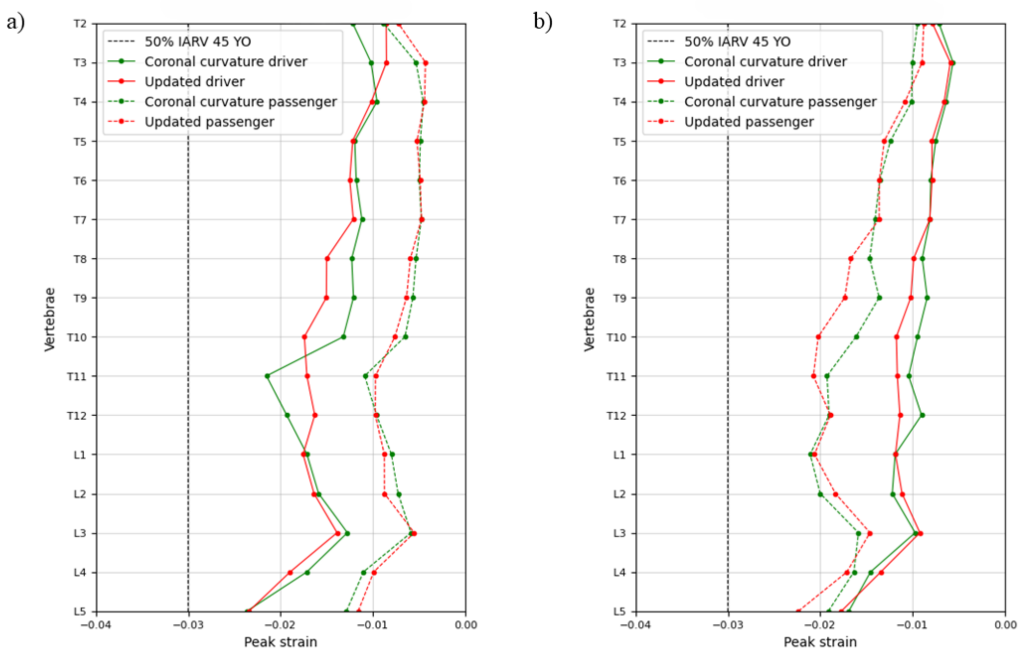

Figure F.1: Peak vertebral strain for updated and coronal curvature a) run-off road (1), b) run-off road (2).

G

Analysis of internal energy

Internal energy of bodily tissues are comprised of potential energy, kinetic energy and thermal energy. Compressive force of a vertebra increases the potential energy of the vertebra, raising the question whether the internal energy was preserved throughout the entire spinal column during impact. To investigate this further, an analysis of the internal energy was performed using ANSA for three FSUs in the run-off road (2) scenario for the passenger, Table G.1. The internal energy of all parts belonging to an FSU were extracted and summed up, i.e. two vertebrae and the intermediate disc.

Table G.1: Internal energy in selected FSUs for run-off road (2) passenger.

FSU	Internal Energy (J)		
	Original	Updated	Coronal Plane
T5/T6	0.38	0.52	0.42
T12/L1	3.50	4.12	3.81
L4/L5	5.05	5.00	4.88

H

Vertebra lamina locations

Table H.1: The coordinates (x,z) of the extracted lamina location for every other vertebra of the original and updated SAFER HBM respectively. The coordinates have been rounded to integers (mm).

Vertebrae	SAFER original	SAFER updated
C3	(-196,567)	(-210,568)
C5	(-196,537)	(-213,538)
C7	(-204,506)	(-222,506)
T2	(-213,468)	(-234,470)
T4	(-227,427)	(-242,423)
T6	(-235,377)	(-244,373)
T8	(-232,324)	(-238,321)
T10	(-221,266)	(-219,264)
T12	(-203,202)	(-191,203)
L2	(-166,147)	(-164,151)
L4	(-130,88)	(-132,90)
S1	(-128,8)	(-133,10)

DEPARTMENT OF MECHANICS AND MARITIME SCIENCES
CHALMERS UNIVERSITY OF TECHNOLOGY
Gothenburg, Sweden
www.chalmers.se